Phys. Med. Biol. **56** (2011) R1–R29 doi:10.1088/0031-9155/56/1/R01

TOPICAL REVIEW

Imaging the elastic properties of tissue: the 20 year perspective

K J Parker[1], **M M Doyley**[1] **and D J Rubens**[2]

[1]Department of Electrical and Computer Engineering, University of Rochester, Hopeman Engineering Building, Box 270126, Rochester, NY 14627, USA
[2]Department of Imaging Sciences, University of Rochester Medical Center, 601 Elmwood Avenue Room, Box 648, Rochester, NY 14642, USA

E-mail: parker@seas.rochester.edu

Received 30 July 2010, in final form 16 September 2010
Published 30 November 2010
Online at stacks.iop.org/PMB/56/R1

Abstract
After 20 years of innovation in techniques that specifically image the biomechanical properties of tissue, the evolution of elastographic imaging can be viewed from its infancy, through a proliferation of approaches to the problem to incorporation on research and then clinical imaging platforms. Ultimately this activity has culminated in clinical trials and improved care for patients. This remarkable progression represents a leading example of translational research that begins with fundamentals of science and engineering and progresses to needed improvements in diagnostic and monitoring capabilities applied to major categories of disease, surgery and interventional procedures. This review summarizes the fundamental principles, the timeline of developments in major categories of elastographic imaging, and concludes with recent results from clinical trials and forward-looking issues.

(Some figures in this article are in colour only in the electronic version)

1. Introduction

Roughly 20 years have elapsed since the production of the first images depicting the local elastic properties of tissues. The first decade of development produced a remarkable proliferation of techniques and optimization strategies. The second decade continued this trend, but with the important extension to dedicated platforms for conducting clinical trials in the hands of radiologists and skilled clinicians. This review focuses on the evolution of the field from basic physics and engineering to clinical trials. Our approach is to highlight major milestones and place them in an overall context, in time and in terms of the underlying biomechanics. The review begins with some brief background on the governing linear equations of motion that form the basis for imaging estimators (section 2). Section 3 covers some of the landmark work in tissue motion and Doppler analyses leading up to the era of imaging. Then, a history of major elastographic imaging approaches is outlined in section 4, as depicted in figure 1.

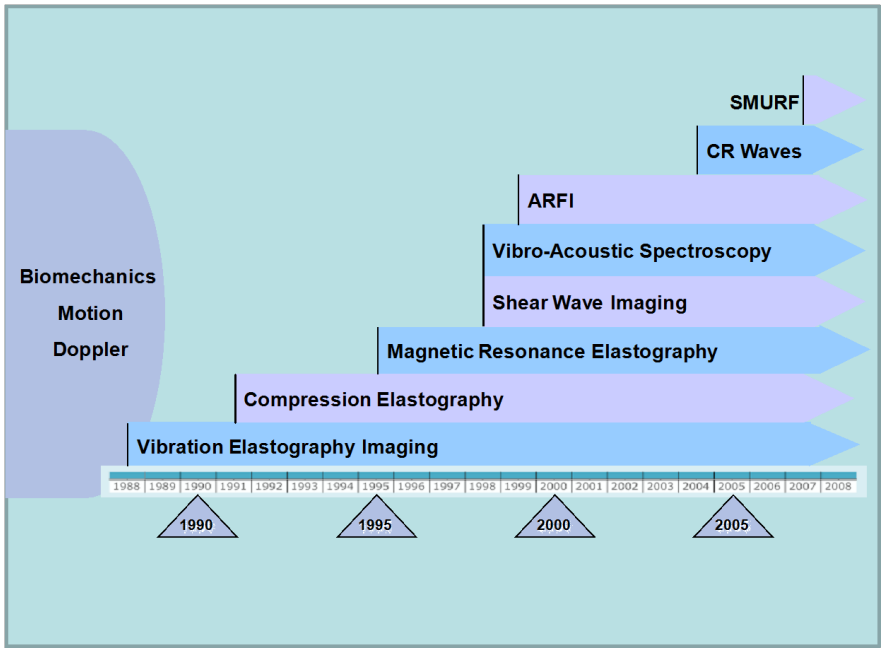

Figure 1. Twenty year timeline of the evolution of elastographic imaging, showing some of the major categories of approaches. Each category is described in detail in section 4.

Finally, some benchmark clinical results are presented in section 5 and directions for future work are highlighted in section 6.

We cannot, unfortunately, attempt an exhaustive review as the number of publications related to the elasticity of liver, as one example, number over 1000. For further study of the topic, one can also reference earlier reviews of the topic (Gao *et al* 1996, Greenleaf *et al* 2003, Parker *et al* 1996, 2005, Sarvazyan *et al* 1995, Garra 2007, Ophir *et al* 1999), and current research results are well represented in the annual International Elasticity Conference (www.elasticityconference.org) and special sessions of the AIUM, ASA, SPIE and RSNA. We also do not review the mathematics of inverse solutions and estimators; these complex issues are beyond the scope of this paper and are left for a later review.

2. Overview of governing principles

The techniques that comprise elastography rely on basic relations that govern displacement and motion of tissues. These can be summarized in a few key governing equations.

The conservation of linear momentum, a fundamental accounting of forces, deformations and acceleration, is derived for a deformable medium using the methods of continuum mechanics, and in integral form applied to some volume:

$$\frac{d}{\mathrm{d}t}\iiint_V \rho\dot{\mathbf{u}}\,\mathrm{d}V = \iint_S \mathbf{T}^{(\mathbf{n})}\,\mathrm{d}S + \iiint_V \rho\mathbf{b}\,\mathrm{d}V. \tag{1}$$

This equation states that the rate of change of linear momentum is equal to the resultant applied surface and body forces. In this equation, ρ is the density, $\mathbf{u}$ is the displacement vector (with the superposed dot indicating a time derivative), $\mathbf{b}$ is the body force per unit mass vector and $\mathbf{T}^{(\mathbf{n})}$ is the traction vector on the surface S (with outward unit normal $\mathbf{n}$) of volume V (Parker *et al* 2005).

Writing the traction vector in terms of the stress tensor σ as

$$\mathbf{T}^{(\mathbf{n})} = \sigma \cdot \mathbf{n}, \tag{2}$$

we can use the divergence theorem to obtain the differential form of conservation of linear momentum, using the dot convention to denote a time derivative:

$$\rho \ddot{\mathbf{u}} = \nabla \cdot \sigma + \rho \mathbf{b}. \tag{3}$$

In measurements of elastic properties, the body forces (such as gravity) are either negligible or their effects can be subtracted from the measured response. Therefore, the last term will not be considered further in this discussion.

To complete the problem statement, the material behavior must be specified. If the deformation is small enough, it can be expressed in terms of the infinitesimal strain tensor:

$$\varepsilon_{ij} = \frac{1}{2}\left(\frac{\partial u_i}{\partial x_j} + \frac{\partial u_j}{\partial x_i}\right). \tag{4}$$

Then, the constitutive relation relating stress and strain for a linear-elastic, isotropic medium can be written as

$$\sigma_{ij} = \left(2\mu\varepsilon_{ij} + \lambda\varepsilon_{kk}\delta_{ij}\right) = \frac{E}{(1+\nu)}\left(\varepsilon_{ij} + \frac{\nu}{1-2\nu}\varepsilon_{kk}\delta_{ij}\right), \tag{5}$$

where λ and μ are called the Lamé constants, μ is also the shear modulus, E is the elastic or Young's modulus and ν is Poisson's ratio. In this equation, the summation convention has been used and δ_{ij} is the Kronecker delta equal to 1 if $i = j$ and 0 otherwise.

In homogeneous regions, where λ and μ are constant, equations (3)–(5) can be combined to obtain an equation in terms of the displacement vector alone as

$$(\lambda+\mu)\frac{\partial^2 u_j}{\partial x_j \partial x_i} + \mu\frac{\partial^2 u_i}{\partial x_j \partial x_j} = \rho\ddot{u}_i, \quad \text{or} \quad (\lambda+\mu)\,\nabla\,(\nabla\cdot\mathbf{u}) + \mu\nabla^2\mathbf{u} = \rho\ddot{\mathbf{u}}, \tag{6}$$

where the body forces, such as gravity, have been assumed to be negligible. This equation, with given boundary and initial conditions, governs the general dynamic response of a homogeneous, isotropic, linearly elastic material to a force or displacement excitation. If loads are applied slowly (quasi-statically) or if the displacement response to a constant load is measured after all the motion has stopped, then the right-hand side of this equation is negligible and set equal to zero. Therefore, this equation governs the static, quasi-static and dynamic (transient, harmonic and wave propagation) responses that can occur in response to applied loads.

The lossy nature of biological tissues is often modeled using a visco-elastic model (Fung 1984) and the simplest models incorporate spring and dashpot elements. The viscous response of a dashpot introduces a time varying term into the constitutive equation. Such a model can be implemented in these equations for a time-harmonic excitation by assuming that λ and μ are complex and frequency dependent. In this case, the wave or vibration amplitude will decay with the distance from the excitation point, and the loss will generally increase with increasing frequency. For a more in-depth presentation of the derivation and solution of the elastic and visco-elastic equations, see Kolsky (1953) and Achenbach (1973).

In many cases it is convenient to represent the response in terms of waves propagating within the tissue. Two types of plane wave, shear waves and pressure waves, propagate independently in the bulk material, interacting only at boundaries. The shear wave equation can easily be obtained from equation (6) by noting that there is no volume change as layers of material move in shear, transverse to the direction of propagation, so the dilatation $\nabla \cdot \mathbf{u} = 0$. The shear wave equation is then

$$\nabla^2\mathbf{u} = \frac{1}{c_s^2}\ddot{\mathbf{u}}, \tag{7}$$

where the shear wave speed is

$$c_s = \sqrt{\frac{\mu}{\rho}}. \tag{8}$$

This equation can either be solved in terms of standing waves or propagating waves, depending on the particular conditions.

Propagating plane pressure waves are irrotational, that is, $\nabla \times \mathbf{u} = \mathbf{0}$ so $\mathbf{u}$ can be written in terms of a potential as $\mathbf{u} = \nabla\psi$. Using the vector identity $\nabla^2\mathbf{u} = \nabla\nabla \cdot \mathbf{u} - \nabla \times \nabla \times \mathbf{u}$, we can obtain the wave equation for $\nabla\psi$ as

$$\nabla^2(\nabla\psi) = \frac{1}{c_p^2}(\ddot{\nabla}\ddot{\psi}), \tag{9}$$

and the pressure wave speed is

$$c_p = \sqrt{\frac{\lambda + 2\mu}{\rho}}. \tag{10}$$

For typical biomaterials, the pressure wave speed is orders of magnitude faster than the shear wave speed. Consistent with this statement, biological tissues are nearly incompressible with $0.49 < \nu < 0.5$. In the limit as ν approaches 0.5, the shear modulus becomes

$$\mu = \frac{E}{2(1+\nu)} \rightarrow E/3. \tag{11}$$

Therefore, for a nearly incompressible material, a measurement of the shear wave speed $c_s \approx \sqrt{E/3\rho}$ can be used to obtain information about the stiffness of the material. Therefore, in elastographic imaging experiments, the focus of attention is typically on the shear wave properties and not on compressional pressure wave properties, which have already been investigated extensively in ultrasonic tissue characterization studies.

Equation (6) can also be a starting point for the consideration of step-compression elastography experiments. For static displacement or very low frequency cyclic motion, the inertial terms are negligibly small. And for nearly incompressible biomaterials, the divergence (or dilatation) $\nabla \cdot \mathbf{u}$ is nearly zero, so equation (6) reduces to Laplace's equation:

$$\nabla^2\mathbf{u} = \mathbf{0}. \tag{12}$$

Solutions to Laplace's equation depend on and reach their extrema on the boundary values of $\mathbf{u}$. For simple one-dimensional geometry the solution for displacement $u_x(x)$ is linear with x, and therefore the strain (the derivative of displacement) is uniform, a fact that is assumed to be true in most step-compression elastographic imaging experiments for homogeneous materials. Deviations from constant strain are indications of local structures that are harder or softer, forming the basis of imaging in compression elastographic methods. Equation (6) is also the starting point for methods that include shear waves, in these cases in the sinusoidal steady state the equation simplifies to equation (7) where the one-dimensional solution to displacement $u_x(x)$ is sinusoidal (Parker *et al* 2005) with a characteristic wavelength λ. The direct estimate of wavelength yields the elastic modulus E using the limiting form of equation (11) for nearly incompressible materials, and this principle forms the basis for many imaging approaches.

While there are an impressive number of approaches to imaging the elastic properties of tissue, it can be emphasized that all techniques lie on a continuum of biomechanical responses. In particular, all simple linear responses of tissue can be captured by equation (6), and this simplifies further due to special conditions such as shear wave excitation (equations (7) and (8)) or quasi-static displacements (equation (12)). In fact the time-dependent terms can be seen as important drivers of the particular response of tissues, and this leads naturally to

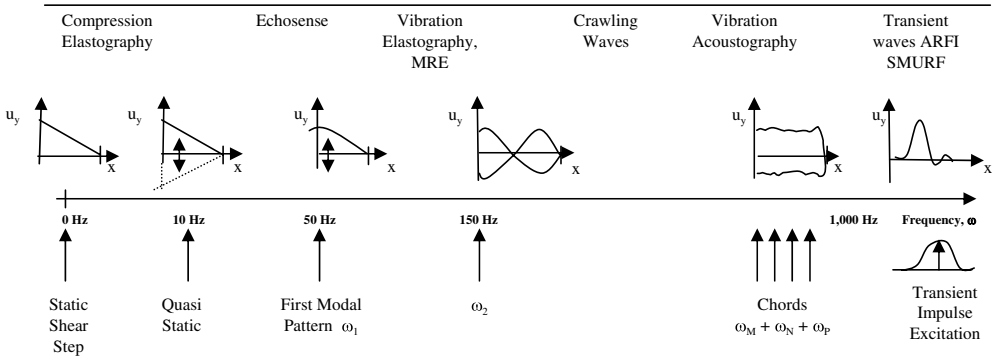

Figure 2. Summary image showing the continuum from step displacement through dynamic vibration and multiple tones. The displacement field u_y is given in each case. The solution for the displacement in the homogeneous object is linear for the static case, sinusoidal for modal patterns at eigen-frequencies, and approaches a constant for multiple, simultaneous 'chord' excitation. Transient waves may be broadband or more narrowband from tone burst excitations.

a continuum, or spectrum, of approaches from very slow motion to sinusoidal steady state motion, to impulsive motion as depicted in figure 2. An overview of the continuum analysis is given in Parker *et al* (2005).

3. Background studies of tissue motion

Oestreicher and colleagues (Oestricher 1951, Von Gierke *et al* 1952) studied the behavior of the human body surface subjected to sound fields or mechanical vibration. They used a strobe light and photography to acquire surface wave propagation patterns, thus obtaining the wavelength and wave speed. They also formulated a theory to explain the increase of impedance of tissue with increasing frequency. A shear modulus estimate was calculated from their experimental data.

Wilson and Robinson (1982) presented a signal processing technique to measure small displacements of liver tissue caused by aortic pulsation and vessel diameter variations. They obtained radio frequency (RF) M-mode signals, and based on the assumption that the tissue follows points of constant phase, they calculated the velocity of tissue motion from the trajectory of a constant phase point. The integral of velocity over time gave a rough estimate of the displacement.

Dickinson and Hill (1982) used the correlation coefficient between successive A-scans to measure the amplitude and frequency of tissue motion. They set up a correlation parameter to measure the changes of the interrogated region between two successive A-scans. The correlation parameter is unity for stationary tissue and decreases monotonically with increasing tissue motion. Their assumption is that the decorrelation is proportional to the displacement, which is only true for very small displacement. This technique was further developed by Tristam *et al* (1986, 1988) to look at the different responses of normal liver and cancerous liver to cardiac movement. They found some features on the correlation curves to distinguish normal liver from that with tumor. They found that livers with tumors generally have lower maximum values, fewer peaks and greater regularity. De Jong *et al* (1990) used a modified correlation technique to measure tissue motion, where they found the maximum cross-correlation by an interpolation algorithm. The peak location of the cross-correlation function may also be determined by several other methods such as oversampling,

sine-interpolation and fitting other curves like parabolas to the neighborhood of the peak of the cross-correlation function. The method of De Jong *et al* (1990) is limited to narrow-band signals, where the cosine function still represents a good approximation.

Fetal lung elasticity may be an important indicator of pulmonary maturity and has been used to determine if the lungs are developing normally. Birnholz and Farrell (1985) tried to qualitatively determine the stiffness of fetal lung by evaluating ultrasound B-scans, where one can see the compression of lung due to cardiac pulsations. They argued that stiff lung tissue transmits cardiac pulsations moving as a block without regional deformation, whereas soft lung tissue compresses, with maximal deformation immediately adjacent to the heart. Adler *et al* (1989, 1990) arrived at more quantitative estimates. They applied correlation techniques to digitized M-mode images and estimated $\langle r \rangle$, a parameter that characterizes the range of transmitted cardiac motion in fetal lung. The parameter is actually the temporally and spatially averaged systolic to diastolic deformation per unit epicardial displacement.

Eisensher *et al* (1983) applied a 1.5 Hz vibration source to liver and breast tissue and used M-mode ultrasound to look at the induced quasistatic compression. They found that the quasistatic compression response from benign lesions was characteristically sinusoidal, whereas those from malignant tumors tended to be more flat, i.e. more of a nonlinear response.

Krouskop *et al* (1987) reported one of the first quantitative measurements of tissue elasticity using gated pulsed Doppler. The set of equations relating tissue properties and tissue movements reduces to some very simple forms under the assumption of isotropy and incompressibility, and the final problem of finding tissue elasticity reduces to measuring tissue peak displacements and their gradients. A single A-line pulsed Doppler instrument was used in their experiments to measure actual tissue flow at points of interest under external vibrations. They suggested a possible measurement of tissue stiffness in a very small region, i.e. 0.5×0.5 mm.

The Doppler spectrum of the scattered ultrasound signal from a vibrating target is similar to that of a pure-tone frequency modulation (FM) process under certain conditions. It has symmetric side harmonics around the carrier frequency. The spacing of the harmonics is equal to the target vibrating frequency, and the amplitudes of the harmonics are given by successive Bessel functions of the first kind. The expression for the signal is (Taylor 1976)

$$s_r(t) = A \sum_{-x}^{x} J_n(\beta) \cos[\omega_0 t + n(\omega_L t + \ell)]. \tag{13}$$

The modulation parameter β of the Bessel function is proportional to the target vibrating amplitude. ω_0 is the angular frequency of the ultrasound signal, ω_L is the angular frequency of the target vibration and ϕ is the vibration phase.

Holen *et al* (1985) observed this characteristic Bessel-band Doppler spectrum when using Doppler ultrasound to examine unusually oscillating heart valves. The Doppler spectrum changes dramatically when the product of the Fast Fourier Transform time and the frequency of the vibrating target vary from less than unity to larger than unity. When the product was larger than unity, the vibration frequency of oscillating heart valves was determined by the spacing between harmonics in the Doppler spectrum. The vibration amplitude was estimated by counting the number of significant harmonics, as an approximation to the frequency modulated bandwidth, which is proportional to the amplitude of the vibrations.

Cox and Rogers (1987) studied the Doppler ultrasound response of fish auditory organs to a low-frequency sound field. The vibration amplitude of the hearing organ was determined by comparing the ratio of the carrier and the first side band of the Doppler spectrum.

These landmark studies set the foundation for the era of imaging that followed.

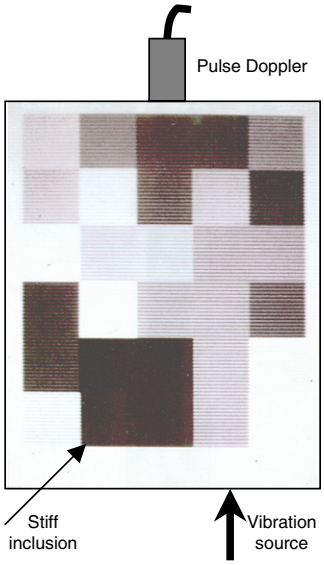

Figure 3. Schematic reconstruction of the first known image of the relative hardness of materials based on Doppler ultrasound signals (see Lerner et al (1988)). The image covers approximately 7 cm vertical × 5 cm horizontal.

4. Imaging techniques

4.1. Vibration amplitude sonoelastography

Dr. Robert Lerner, a radiologist at the University of Rochester, was intrigued by the ability of palpation to detect some prostate cancers that were undetectable by ultrasound. After some experimentation, Lerner and Parker (1987) developed and presented preliminary work on vibration amplitude sonoelastography (sonoelasticity imaging). In vibration amplitude sonoelastography, a low-frequency vibration (20–1000 Hz) is externally applied to excite internal vibrations within tissue under inspection. A stiff inhomogeneity inside surrounding soft tissue produces a disturbance in the normal vibration eigenmode patterns. Doppler detection algorithms are employed to make a real-time vibration image. In some organs, modal patterns can be created, revealing additional information as to the shear wave speed of sound in the tissue (Parker and Lerner 1992).

The first vibration amplitude sonoelastography image, published by Lerner and Parker (1987) and again by Lerner *et al* (1988), is shown in figure 3.

This early image shows the vibration within a sponge containing a hard region (lower dark region). The sponge was vibrated from below, and pulsed, range-gated Doppler was used to determine the vibration amplitude within its interior. By 1990, the University of Rochester group was using a modified color Doppler instrument to make real-time vibration amplitude sonoelastography images, albeit bistable, where vibration above a threshold (approximately 2 μm) produced a saturated red (figure 4).

Tissue elastic constant measurements, sonoelastography finite element modeling results and phantom and *ex vivo* tissue results were reported (Lerner *et al* 1988, 1990, Parker *et al* 1990). Thus, by the end of 1990, the working elements of vibration elastography (sonoelastography and sonoelasticity were other names used at the time) were in place,

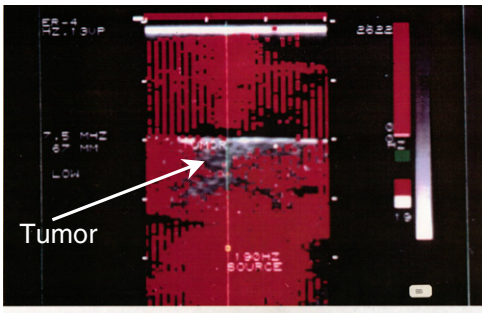

Figure 4. A typical image from the first generation of vibration sonoelastography images, circa 1990. Doppler spectral variance is employed as an estimator of vibration in the 1–10 μm range and displayed over the B-scan images. No color implies low vibrations below the threshold. Shown is the fill-in of vibration within a rabbit liver, with a growing VX2 tumor indicated by the deficit of color.

including real-time imaging techniques and stress–strain analysis of tissues such as prostate, with finite element analyses and experimental images demonstrating conclusively that small regions of elevated Young's modulus could be imaged and detected using conventional Doppler imaging scanners.

By 1992, studies of liver, breast and kidney were published, and a study of *ex vivo* prostate cancer detection was completed (Parker and Lerner 1992, Lee *et al* 1991). In 1994, a real-time *in vitro* study of prostate had been completed, demonstrating that vibration amplitude sonoelastography had better sensitivity and predictive values than did B-scan imaging alone (Rubens *et al* 1995). Furthermore, in 1994 a mathematical model for vibration amplitude sonoelastography was completed (Gao *et al* 1995). A sonoelastic Born approximation was used to solve the wave equations in an inhomogeneous (but isotropic) medium. The total wave field inside the medium can be expressed as

$$\Phi_{\text{total}} = \Phi_i + \Phi_s, \tag{14}$$

where Φ_i is the homogeneous field or incident field and Φ_s is the field scattered by the inhomogeneity. They satisfy, respectively,

$$(\nabla^2 + k)\Phi_i = 0 \tag{15}$$

$$(\nabla^2 + k)\Phi_s = \alpha(x), \tag{16}$$

where $\alpha(x)$ is a function of the properties of inhomogeneity. The theory accurately describes how a hard or a soft lesion appear as disturbances in a vibration pattern. Figure 5 summarizes the theoretical and experimental trends.

Another aspect of vibration amplitude sonoelastography to be considered is the signal processing for estimation of key parameters. Huang *et al* (1990) proposed a technique to estimate the vibration amplitude β from the spectral spread. The simple relationship between β (which is proportional to the vibration amplitude of the target) and the spectral spread σ_ω they found is

$$\beta = \sqrt{2}(\sigma_\omega/\omega_L), \tag{17}$$

where ω_L is the vibration frequency of the vibrating target. This is a simple but useful special property of the Bessel Doppler function. They also investigated the effect of noise, sampling and nonlinearity on the estimation. A later paper by Huang *et al* (1992) extended this work

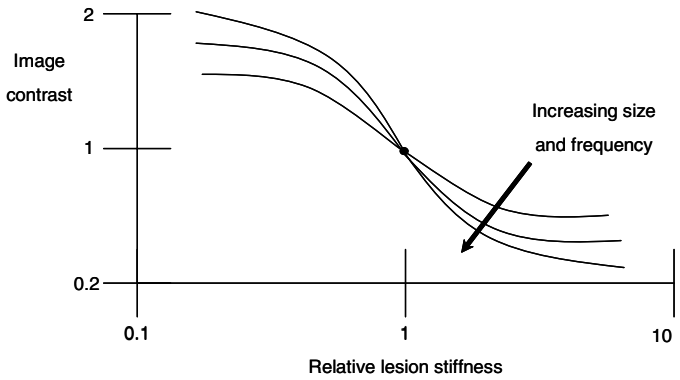

Figure 5. Schematic drawing of theoretical results of the contrast of vibration sonoelastography for soft or hard lesions in a background medium. The image contrast increases with both increasing frequency and increasing size of the lesion.

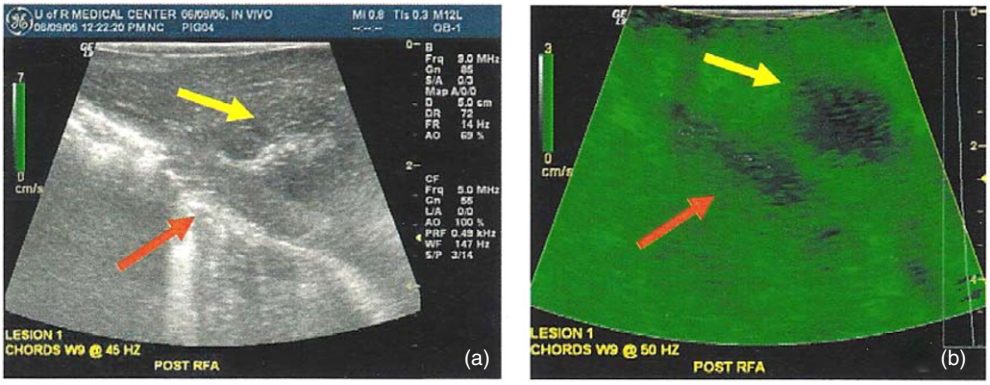

Figure 6. *In vivo* porcine liver with a thermal lesion. The B-scan (a) shows a lesion (yellow arrow) with indistinct boundaries. The sonoelastography image (b) demonstrates a vibration deficit indicating a hard lesion. Red arrows point to boundary of the liver.

to real-time estimators of vibration amplitude, phase and frequency that could be used for a variety of vibration sonoelastography techniques.

Implementations of various time and frequency estimators make this technique a real-time diagnostic tool with applications to both superficial and deep organs (Gao *et al* 1997, Taylor *et al* 2000, 2005, Wu *et al* 2002, Zhang *et al* 2008a, 2008b, Carstensen *et al* 2008, Hoyt *et al* 2008b). An example of *in vivo* imaging of a thermal-induced lesion in porcine liver is shown in figure 6.

The advantage of this technique is that it is compatible with most color Doppler scanners. However, like compression elastography, it produces only a relative image contrast related to local hardness; therefore, it is important to establish a uniform background within an organ. Shear wave losses and modal patterns from reflective boundaries can make this objective difficult in certain situations. Finally, a source of vibration must be added to the scanning system, adding some extra expense to equipment.

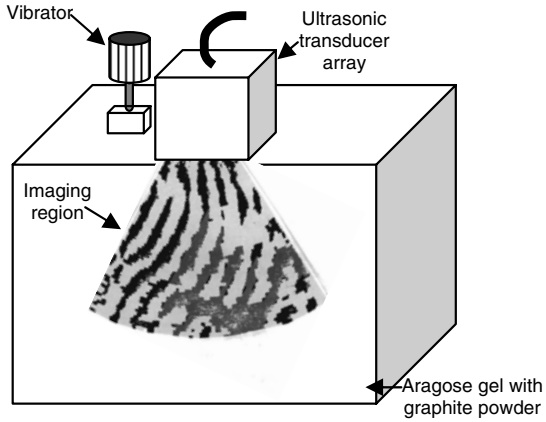

Figure 7. Schematic drawing of the system developed by Professor Sato and colleagues at the University of Tokyo, including external vibration and an imaging array with signal processing for deriving the phase of the vibration in tissue. The rate of change of phase can be estimated to yield tissue hardness.

4.2. Vibration phase gradient sonoelastography

Sato *et al* (1985) were involved with the study of nonlinear interactions between ultrasound and lower frequency waves in tissue at the time that Parker and Lerner, and Krouskop and Levinson were using linear methods to investigate the propagation of vibrations inside tissue. In the late 1980s Sato (Yamakoshi *et al* 1990) developed a vibration phase gradient approach to sonoelastography. His technique maps both the amplitude and the phase of low-frequency wave propagation inside tissue, and from these maps, the wave propagation velocity and dispersion properties are derived. These parameters are directly linked to the elastic and viscous characteristics of tissue.

Because the phase-modulated (PM) Doppler spectrum of the signal returned from sinusoidally oscillating objects is similar to that of a pure-tone frequency modulation (FM) process, the tissue vibration amplitude and phase of tissue motion may be estimated from the ratios of adjacent harmonics.

From equation (13), the amplitude ratio of adjacent Bessel bands of the spectral of the signal is

$$A_{i+1}/A_i = |J_{i+1}\ (\beta)/J_i(\beta\ )|\,. \tag{18}$$

If A_{i+1}/A_i is calculated as a function of β beforehand, then β can be estimated from the experimental data.

Phase and amplitude maps (figure 7) constructed as a function of time permit the display of wave propagation as a moving image.

Images of amplitude and phase are computed offline by using a minimum squared error algorithm to estimate the direction of wave propagation and to calculate phase and amplitude gradients in this direction. Preliminary *in vivo* results have been demonstrated (Yamakoshi *et al* 1990) under the assumption that the effect of shear viscosity is negligible at low frequencies.

Levinson *et al* (1995) adapted and refined Sato's technique (Yamakoshi *et al* 1990) by using a more general model of tissue visco-elasticity and by using a linear recursive filtering algorithm based on cubic B-spline functions. By taking the Fourier transform of the wave

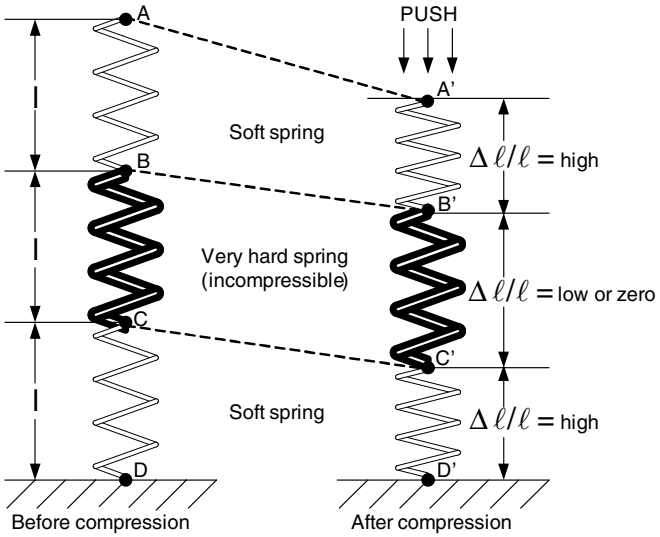

Figure 8. Schematic and conceptual argument used to explain the strain images produced by early compression elastography systems (see Ophir *et al* (1991)).

equation, he found that the frequency domain displacement equation for a linear, homogeneous, isotropic viscoelastic material can be written as

$$-\rho\omega^2 U = (\mu + \mathrm{i}\omega\eta)\ \nabla^2 U + [(\mu + \lambda) + \mathrm{i}\omega(\eta + \kappa)]\nabla\nabla \cdot U, \tag{19}$$

where U is the temporal Fourier transform of the internal tissue displacement, ρ is the density, μ and λ are the shear and longitudinal moduli of elasticity (also known as the Lamé constants) and η and κ are the shear and longitudinal coefficients of viscosity, respectively. This equation can lead to expressions that relate the shear modulus of elasticity and viscosity to the wave number and the attenuation coefficient of the wave.

Using the assumptions that viscosity at low frequencies is negligible and that shear waves predominate, Levinson *et al* (1995) conducted a series of experiments on the quadriceps muscle group in human thighs. The values of Young's modulus of elasticity were calculated from the phase gradient images of the subjects' thighs under conditions of active muscle contraction. A pulley apparatus was used to control the tension applied to the muscle. As expected, the measured speed of vibration propagation and the calculated values of Young's modulus increased with increasing degrees of contraction as needed to counteract the applied load. Phase gradient techniques have the advantage of yielding quantitative estimates of wave speed. Strictly speaking, a 3D mapping of waves is required; however conventional ultrasound scanners provide only a 2D imaging slice.

4.3. Compression elastography

Introduced in 1991 by Ophir *et al* (1991) compression elastography utilizes a comparison of ultrasound B-scan RF information from tissue before and after a modest compression. The concept can be explained by invoking the stress–strain relations under a simple uniaxial (one dimensional) displacement. This was modeled by use of springs, as depicted in figure 8.

In one-dimensional compression, a series of springs will displace according to their relative stiffness—the stiffest spring will compress the least. Thus, by calculating the strain (the derivative of displacement), areas of relative stiffness could be identified and

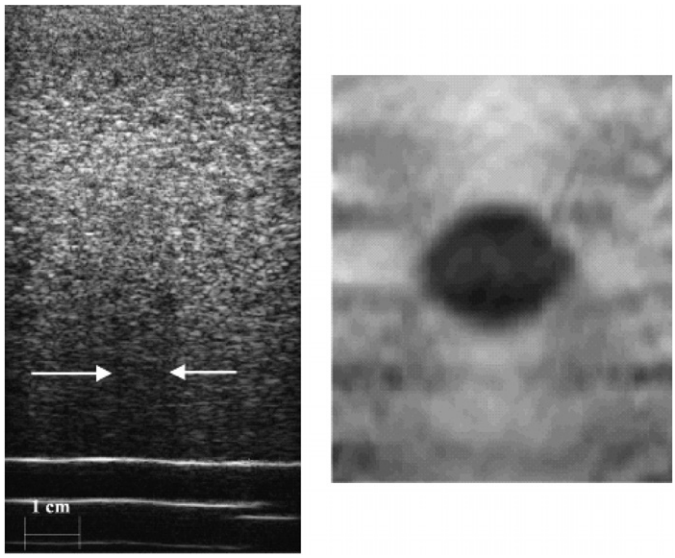

Figure 9. Representative compression elastography displays. Left, a B-scan with embedded isoechoic lesion in a phantom. Arrows point to a subtle shadow below the lesion. Right, a corresponding strain image (zoomed around lesion) demonstrating a dark region of low strain.

imaged as low strain regions, as demonstrated in figure 9. Displacements are estimated by comparing the echoes before and after compression by correlation methods or by other techniques. Compression elastography thus produces images of relative strain which are simple to interpret so long as the applied stress is relatively uniform. The advantage of the technique is that the ultrasound scanning transducer, handheld in most applications, can be used to produce a localized compression near the region of interest in the breast and other applications, particularly in more superficial targets of interest.

The disadvantages include the relative nature of the strain image, the requirement for nearly uniform strain to interpret the image, the tendency of objects to move out-of-plane during compression and the difficulty of compressing deeper organs.

Major engineering efforts have improved the signal processing and systems implementation of compression elastography (Varghese and Ophir 1997, Varghese *et al* 1996, Sumi 2008, Hall *et al* 2003, Shiina *et al* 2002). In addition, efforts have been made to solve the inverse problem and create quantitative estimates of tissue elasticity from models applied to the raw displacement data (Barbone and Gokhale 2004, Fehrenbach 2007). However, the clinical applications currently under investigation are predominantly conducted using compression and interpretation of the resulting relative strain image.

Compression elastography can be implemented on B-scan imagers as real-time-dedicated signal processing or as post-processing of the pre- and post-compression signals. The straightforward implementation has helped to disseminate the approach to a number of platforms including Hitachi, Siemens, Ultrasonix and other scanners (Varghese and Ophir 1997). Research applications include HIFU lesions in liver (Righetti *et al* 1999), prostate (Kallel *et al* 1999), breast (Garra *et al* 1997), RF lesions in liver (Varghese *et al* 2003) and HIFU lesions in the prostate (Curiel *et al* 2005). Extensions of compression elastography include poroelastic imaging with time-dependent behavior of complex media (Berry *et al* 2006) and shear–strain elastography (Thitaikumar *et al* 2007). Clinical applications are covered in section 5.

4.4. Magnetic resonance elastography

Elastography can be performed using magnetic resonance imaging (MRI), and despite the comparatively long acquisition times (15 min per direction) magnetic resonance elastography (MRE) has also shown promise in the detection and differential diagnosis of breast (Kruse *et al* 2000, Lorenzen *et al* 2001, McKnight *et al* 2002, Van Houten *et al* 2003) and prostate (Kemper *et al* 2004) cancer, monitoring minimally invasive therapeutic techniques (Wu *et al* 2000) and characterizing the mechanical properties of brain (McCracken *et al* 2005) and plantar (Weaver *et al* 2005).

MRI is more expensive than diagnostic ultrasound, but it can measure all three spatial components of the induced tissue displacement with high accuracy and precision, and thus is more suited for quantitative elastography (Manduca *et al* 1998, 2001, Samani *et al* 2003, Tikkakoski 2007, Van Houten *et al* 2001, Weaver *et al* 2001). Consequently, several groups actively developed MRE; like its ultrasound counterpart, MRE visualizes the mechanical properties within soft tissues by employing either a quasi-static or dynamic mechanical source (Kruse *et al* 2000, Weaver *et al* 2001, Muthupillai *et al* 1997, Plewes *et al* 2000, Sack *et al* 2004, Sinkus *et al* 2007). However, in MRE the induced tissue motion is measured using either the saturation tagging (Axel and Dougherty 1989, Zerhouni *et al* 1988) or the phase-contrast method.

4.4.1. Quasi-static MRE. Fowlkes *et al* (1995) proposed a quasi-static approach to MRE that measures internal tissue strain using the saturation tagging method. Although encouraging strain elastograms were produced with this technique the spatial resolution of images is questionable. Plewes and colleagues (Bishop *et al* 1998, Hardy *et al* 2005, Plewes *et al* 1995) proposed an MRE method that utilizes a phase-contrast imaging sequence to estimate the spatial strain incurred when the tissue or phantom under investigation is deformed quasi-statically. They conducted phantom studies, which support the results observed in quasi-static ultrasound elastography (Bamber *et al* 2002, Bamber and Bush 1996, O'Donnell *et al* 1994, Ophir *et al* 1997). More specifically, high contrast focal lesions are discernable in strain elastograms. They also proposed to reconstruct the intrinsic tissue mechanical properties using an iterative inverse image reconstruction method (Bishop *et al* 2000).

4.4.2. Dynamic MRE. Muthupillai *et al* (1995) proposed a dynamic approach to MRE based on the phase contrast imaging method. They modified a standard spin echo imaging sequence, by introducing a motion-sensitizing MR gradient in a specific direction, whose polarity was switched repeatedly at a defined frequency. They induced shear waves within the tissue under investigation at the same frequency as the motion-encoding gradient with a harmonic mechanical source that was coupled to the surface. The cyclic motion of nuclear spins produces a phase shift ϕ in the received MR signal when the motion-sensitizing gradient is applied. The resulting phase shift is given by

$$\phi(r,\theta) = \frac{2\gamma NT(\vec{G}\cdot\vec{\xi}_0)}{\pi}\sin(k\cdot\vec{r}+\theta), \tag{20}$$

where $\vec{\xi}_0$ represents the displacement amplitude vector, $\vec{G}$ represents the motion-sensitizing magnetic gradient vector, θ represents the relative phase between the mechanical source and magnetic oscillations, γ represents the gyro magnetic ratio and is the spin position vector, $\vec{r}$ represents the mean position, k represents the wave vector, T represents the period of the mechanical excitation and N represents the number of gradient cycles. Spins will have maximum phase shifts of opposing polarities when their component of motion are in the

direction of the gradient vector; and spins will have no net phase shift when their component of motion is 90° degrees out of phase with the magnetic gradient vector. Muthupillai *et al* (1995) demonstrated using phantoms and excised tissue samples that propagating shear waves can be visualized at a high spatial resolution. Like sonoelasticity imaging, the shear modulus can be computed directly from local estimates of wavelength. Although this technique is very elegant in terms of its simplicity, accurate quantification of wavelength in complex organs such as the breast can be difficult; therefore, Muthupillai and colleagues computed the shear modulus by applying the local frequency estimation (LFE) technique (Manduca *et al* 1996) to MRE data, which has produced encouraging *in vivo* and *in vitro* results despite its origin as an imaging processing technique (Kruse *et al* 2000, 2008, Dresner *et al* 1998).

4.4.3. Steady-state harmonic MRE. Two groups (Sinkus *et al* 2000, Weaver *et al* 2000) proposed independently an alternate approach to MRE that measured the mechanical properties of soft tissue under steady state harmonic excitation. Like the MRE approach described by Muthupillai *et al* (1995) this method also employed the phase-contrast imaging method. The main difference between the two approaches is the method used to reconstruct shear modulus. Sinkus *et al* (2000) proposed a direct inversion scheme where the elastic properties (e.g. shear modulus and Poisson's ratio) were calculated using a system of partial differential equations in which the spatial derivatives of the measured displacements appears as coefficients. This technique is very appealing because it is linear, efficient and can be localized under the assumptions of piecewise homogeneity in the mechanical properties. However, the technique is also very sensitive to measurement noise, which is not surprising since significant noise amplification occurs when the measured data are differentiated. Consequently, the measured displacements and/or their spatial derivatives must be filtered to stabilize performance in practice.

Weaver *et al* (2001) computes shear modulus from time harmonic tissue displacements using an iterative inversion technique that does not require data differentiation (Van Houten *et al* 1999, 2001). While this method may be less sensitive to measurement noise, its utility is hampered by the large computational overhead which is required to solve the three-dimensional inverse elastography problems on a highly resolved finite element mesh, which the group overcame by implementing their overlapping subzone inversion technique (Van Houten *et al* 1999) on a parallel computing platform (Doyley *et al* 2004). Very encouraging phantom and patients studies have been reported with the technique, as demonstrated in figure 10.

4.5. Radiation force vibration acoustography

As an ultrasound beam propagates through an absorbing medium, the energy transfer results in a second-order effect that produces a force proportional to local intensity and absorption, which is termed radiation force (Torr 1984). In 1990, Sugimoto *et al* (1990) devised a laboratory system that applied radiation force to a tissue sample, while measuring the resulting displacement with an ultrasonic probe. The displacement versus time relaxation curve was fit to a multi-exponential function as a model of the mechanical properties (figure 11).

Fatemi and Greenleaf (1998) developed a two-frequency strategy with co-incident foci to create images of tissue response. The second-order (intensity) physics of radiation force produce a difference frequency term which would produce an oscillating body force on a prescribed region, with the difference frequency controllable and typically in the low KHz range or less. By raster scanning the coincident beams, a region of interest could be scanned and a separate hydrophone, tuned to the difference frequency, was used to estimate the response of the objects or tissues. Spectroscopic information can be obtained by varying the difference

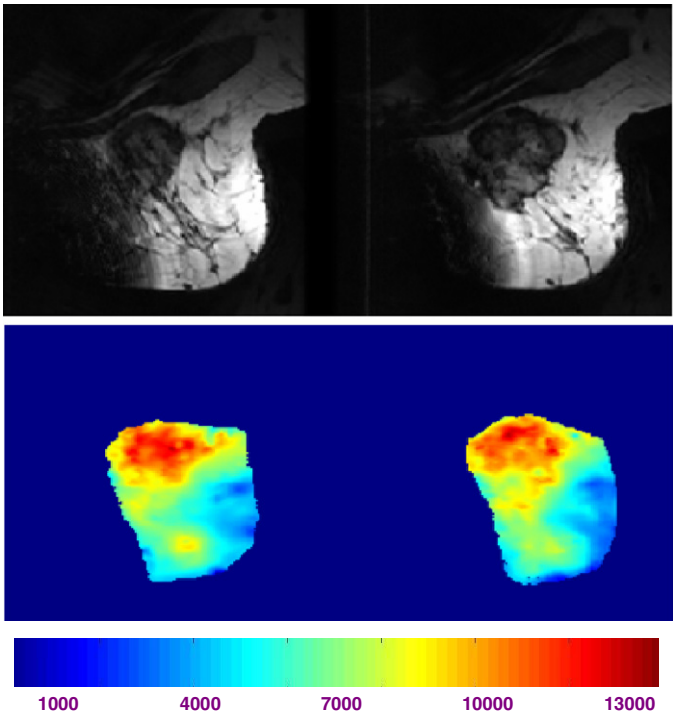

Figure 10. Representative MRE studies of the breast. Top: the MR study of a patient before and after chemotherapy. Bottom: quantitative estimates of elasticity based on MRE of the same areas of interest, at both time points. A reduction of the highest values of stiffness is noted after chemotherapy. (Courtesy of Drs K Paulsen and J Weaver, Dartmouth College.)

frequency over some bandwidth. The technique has been applied to a variety of targets including vessels, phantoms, lesions and contrast agents (Fatemi and Greenleaf 1998, 1999, Fatemi *et al* 2002, Mitri *et al* 2009, Urban *et al* 2006, Chen *et al* 2007, Zhang *et al* 2007b). Konofagou and Hynynen (2003) have devised a localized harmonic imaging (HMI) using an amplitude modulated focused beam, for the detection of localized stiffness.

4.6. Transient shear wave imaging

A number of techniques focus on the propagating wave that results from a transient (impulsive or short tone burst) excitation of the tissue. Sarvazyan *et al* (1998) proposed a method based on acoustic radiation force generated shear waves. The local propagation from a focus was analyzed to estimate the local shear parameters (figures 12 and 13).

Nightingale *et al* (2006), Wang *et al* (2007) and Palmeri *et al* (2007) conducted related studies in the liver to ascertain the degree of liver fibrosis.

Separately, Catheline *et al* (1999) devised a low frequency (50 Hz) external mechanical vibrator integrated with an ultrasound M-mode system. This integrated applicator can be applied through the ribs to excite a short tone burst which propagates into the liver. The ultrasound tracking provides a displacement history along the axial center line, and from this a global estimate of liver shear velocity and thus elasticity can be estimated. This technique is implemented in a stand-alone clinical device, the Fibroscan manufactured by Echosense

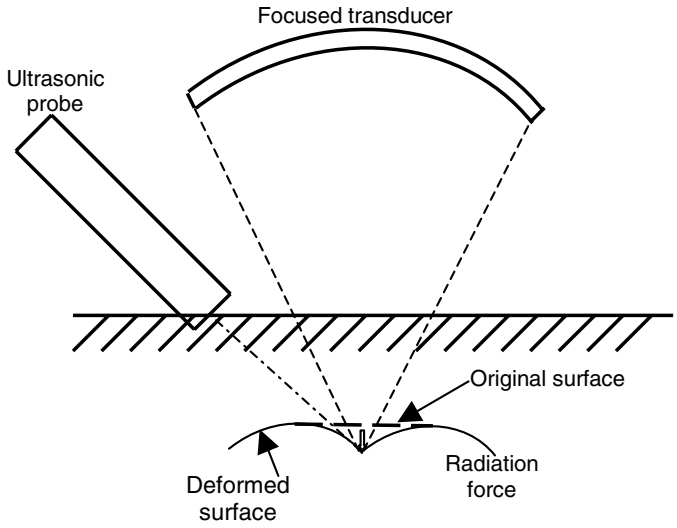

Figure 11. Schematic representation of the early work by Sugimoto to measure the displacement of a specimen's surface under radiation force.

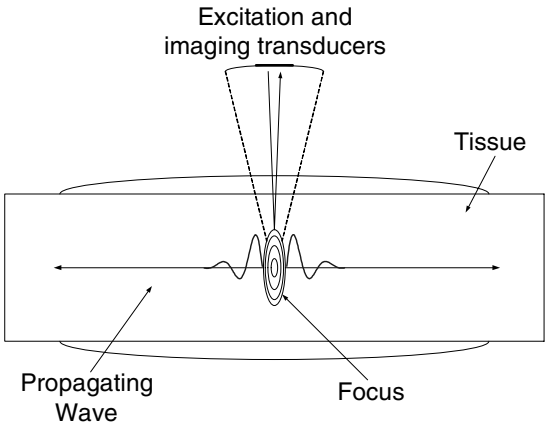

Figure 12. Schematic concept representing the explanation of shear wave measurements from a focused beam imparting a radiation force excitation to tissue.

in France, and is unique in that it does not require integration into a conventional imaging system.

Bercoff *et al* (2004) developed an ultra high speed (10 000 imaging frames per second) ultrasound scanner that was capable of monitoring the wave propagating from an ARF impulse within the tissue. Multiple ARF impulses fired at a rapid rate compared to the relatively slow shear wave speed were termed 'supersonic' excitations and are implemented in a supersonic shear imaging scanner. This approach has been used to study the viscoelastic properties of breast lesions (Tanter *et al* 2008), muscles (Deffieux *et al* 2007b) and liver (Deffieux *et al* 2007a).

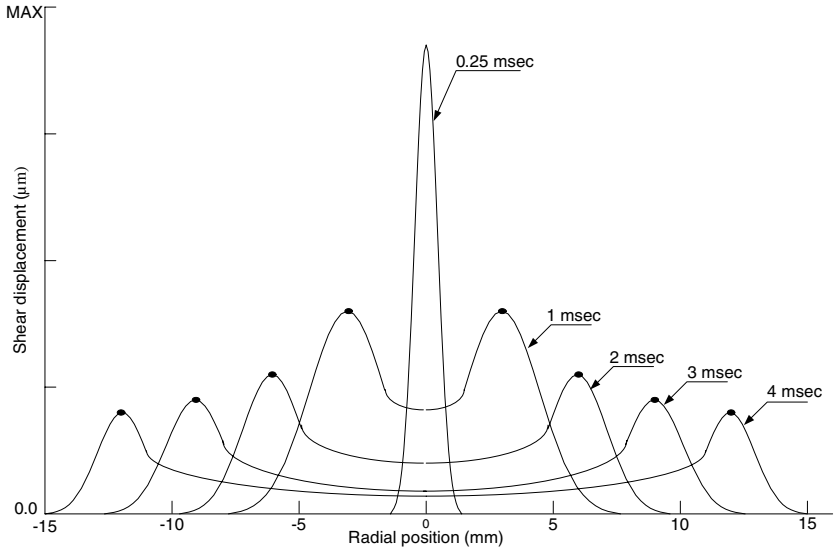

Figure 13. Schematic concept of the time-space evolution of displacements in tissue caused by a short radiation pulse excitation. An initial displacement (center) spreads progressively as depicted at 1 ms, 2 ms, and subsequent intervals.

More recently, McAleavey *et al* have devised a method named spatially modulated ultrasound radiation force (SMURF) (McAleavey and Menon 2007). Instead of utilizing a sharp focal region to deliver an impulse of ARF to the tissue, a spatially modulated pattern is employed to set up a unique spatial frequency within a region of tissue. After excitation of this spatial frequency with an impulse of ARF, the temporal history of displacements are obtained and analyzed to estimate the local shear wave speed. This technique has been validated in tissue-mimicking phantoms (McAleavey *et al* 2009).

4.7. Acoustic radiation force imaging

The use of acoustic radiation force (ARF) as an imaging modality was introduced by Nightingale *et al* (1999, 2001) ARFI provides multiple parameters and strategies, for example one can map the maximum displacement as points are successively pushed, or the relaxation time following each push. The technique has been demonstrated in breast (Sharma *et al* 2004), prostate (Zhai *et al* 2010) and for delineation of RFA lesions (Fahey *et al* 2004, 2005). An example of prostate ARFI is given in figure 14.

The advantages of ARFI (and the other radiation force based techniques) stem from the fact that anywhere an imaging system can focus; a pushing pulse of radiation force can be applied. The disadvantages are that ARF is a relatively weak effect, thus high intensities and heating of the system and tissue place limits on the resulting displacements (Palmeri and Nightingale 2004).

4.8. Crawling wave imaging

More recently, Wu *et al* (2004, 2006) used sonoelastography to image slowly moving interference patterns, termed crawling waves, produced by two opposing shear vibration sources with a slight difference in frequency or phase. The University of Rochester group

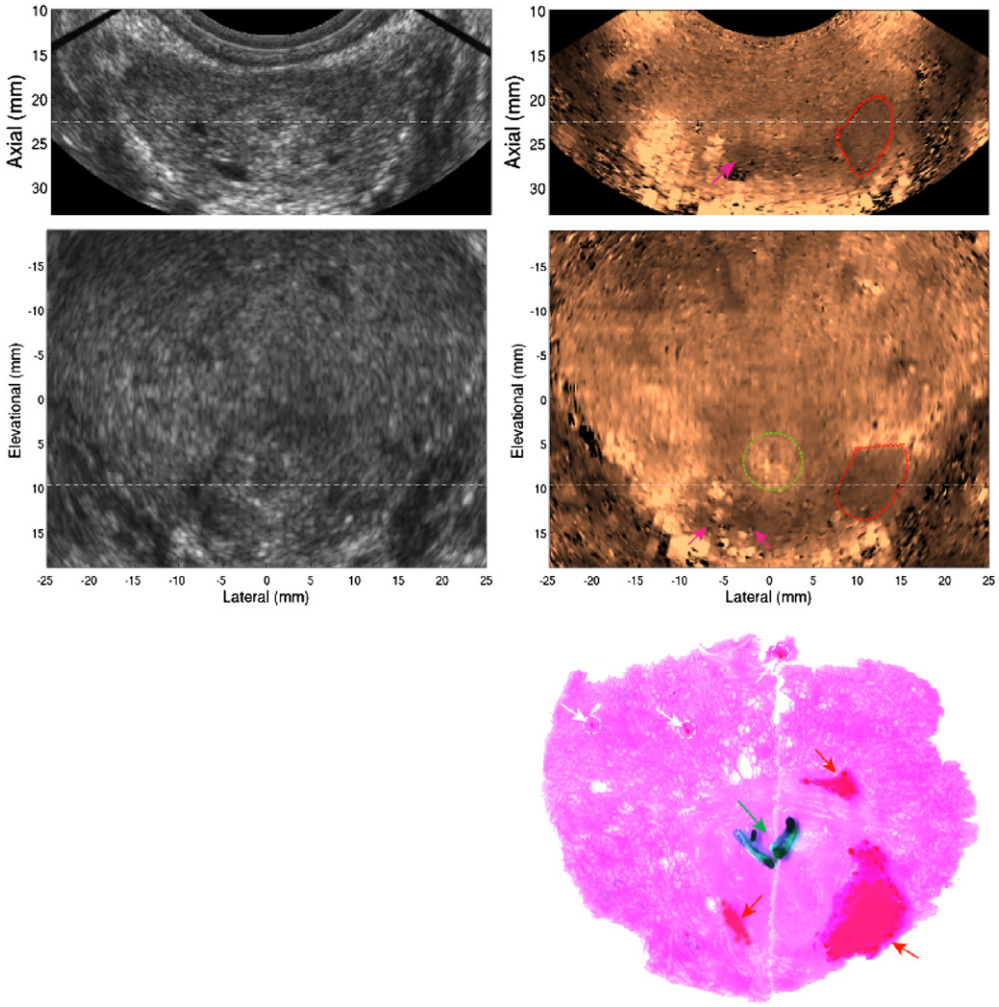

Figure 14. Matched 3D B-mode and ARFI images obtained *in vivo* immediately prior to surgical excision of the prostate in a patient with known prostate cancer, in axial (top row) and coronal views (second row) with the corresponding coronal view of the H&E-stained histologic slides (bottom row). The two imaging planes intersect at an angle of about 60° at the dashed lines. In ARFI images, darker regions correspond to regions of decreased displacement in response to the acoustic radiation force (i.e. stiffer structures). In reviewing prostate ARFI data, regions suspicious for cancer appear darker than their surrounding tissue, and asymmetric in both coronal and axial views. Histologically confirmed suspicious regions of PCa are circled with red dashed lines in the ARFI images, additional suspicious cancerous regions are indicated by magenta arrows and the verumontanium is circled with green lines. In the histological images (third row), the cancerous regions (Gleason's score 4+3) are masked in red and the verumontanium is masked in dark green. Small PCa foci (less than 1 mm) are circled with white dashed lines. (Courtesy of Drs K Nightingale and L Zhai, Duke University.)

determined that the local velocity of the crawling waves is proportional to the underlying local shear velocity which in turn can be used to estimate the elasticity modulus of the tissue. The estimation of the local shear velocity can be performed using local frequency estimators, a technique imported from MRE. Other estimation techniques have been proposed by McLaughlin *et al* (2007) and Hoyt *et al* (2007b, 2008a) based on arrival times and

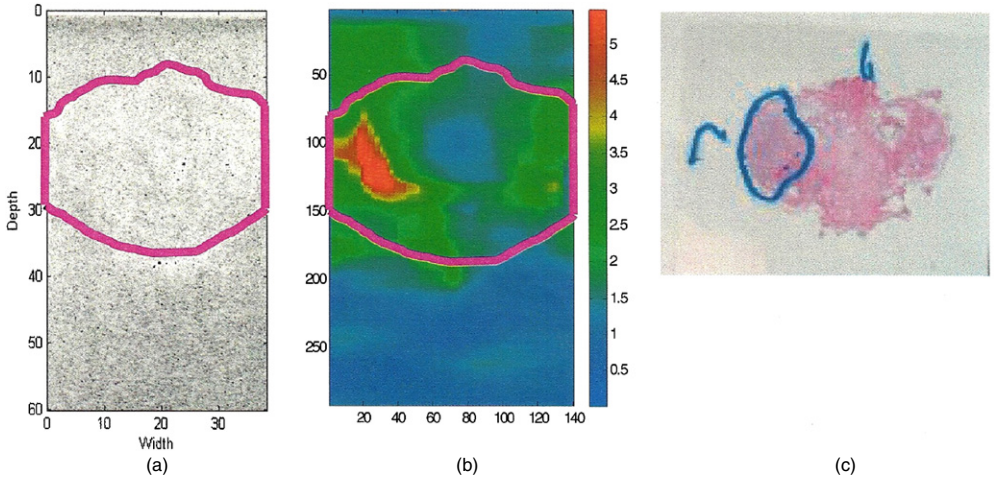

Figure 15. Corresponding B-mode (a), shear speed estimates from crawling waves (b) and histological (c) images of a cross-section close to the apex of a human prostate gland. The boundary of the prostate gland is shown in pink. The shear speed image shows a region with elevated shear speed on the left side of the cross-section which corresponds to a cancerous region in the histological image. (Courtesy of Professor B Castaneda.)

autocorrelation methods, respectively. Crawling wave sonoelastography has been successfully applied to detect radio frequency ablated hepatic lesions *in vitro* (Hoyt *et al* 2008a, Zhang *et al* 2007a), to characterize human skeletal muscle *in vivo* (Hoyt *et al* (2007a, 2008c)) and to characterize human prostate tissue *ex vivo* (Castaneda *et al* 2009). An example is shown in figure 15.

4.9. Other related techniques

In principle, it is possible to utilize any tomographic imaging system to track tissue motion and deduce some biomechanical properties of the tissue. The evolution of the elastographic imaging techniques covered in previous sections relied mostly on ultrasound and MRI. However, optical systems can be configured to track tissue motion in real time. In particular, optical coherence tomography (OCT) is directly analogous to ultrasound imaging in that a speckle image of a 2D plane can be produced at high frame rates. Penetration in tissue of the optical wavelengths is limited but within the imaging plane, tissue motion can be tracked using correlation techniques or Doppler techniques that parallel those used in ultrasound. Compression elastography by OCT was introduced by Schmitt (1998) using a free-space Michelson interferometer and utilizing speckle tracking to determine displacements and then calculate strain. Other work employs a variety of Doppler and correlation methods to track the response of tissues (Wang *et al* 2006, Kirkpatrick *et al* 2006, Liang *et al* 2008, 2010, Kennedy *et al* 2009). The advantage of optical methods is that very high resolution and microscopic studies can be performed.

A distant relative of elastographic imaging is the field of thermo-acoustic imaging, which has largely developed independent of the methods covered in section 4. In thermo-acoustic imaging, a short impulse of electromagnetic energy or laser energy is distributed throughout a tissue, and differential absorption creates thermal expansion waves which are detected and utilized in a reconstruction (Patch and Scherzer 2007). Both EM-acoustic imaging (Bowen 1981, Bowen *et al* 1981, Nasoni *et al* 1985) and opto-acoustic imaging (Oraevsky *et al* 1999,

Esenaliev *et al* 1999) have been actively developed over the last few decades. At a high level of abstraction, these techniques, like elastographic techniques, attempt to reconstruct the differential response of tissues to an input. The fusion of these techniques has been explored by Emelianov *et al* (2004).

5. Clinical results

Over the past several years elastography has moved out of the laboratory and into the hands of clinicians. The most rapidly adopted areas include liver, breast, prostate and thyroid. Liver elastography has become a mainstay for gastroenterologists who use a non-imaging instrument (Fibroscan) to assess liver parenchymal stiffness in patients with hepatitis, at risk for developing cirrhosis. Calculations of liver stiffness based on transient elastography (Fibroscan) have shown better than 90% correlation with Metavir staging for hepatitis C and have a better than 90% negative predictive value for cirrhosis (stage 4 disease) (Wang *et al* 2009). When Fibroscan is combined with a blood test for liver fibrosis (fibrometer) sensitivity and specificity rise to over 90% for advanced (stage 4) disease (Boursier *et al* 2009). One of the limitations of current liver elastography is that it has no imaging component. A second difficulty involves depth of penetration as well as liver contact. Very large patients and/or patients with ascites are not as effectively studied, with one in five obese patients having inadequate studies (Castéra *et al* 2008, 2010). New equipment and processing techniques are being developed to overcome these limitations.

Imaging of more superficial structures has been more successful. The most widely adopted application in the USA has been breast compression elastography. A direct compression technique has become commercially available from multiple manufacturers, and the sensitivity and specificity for carcinoma versus benign disease are above 95% and 80%, respectively (Ginat *et al* 2009, Barr 2006, Thomas *et al* 2007). In a multicenter study from Wojcinski *et al* (2010) assessing 779 patients, elastography demonstrated an improved specificity (89.5%) and an excellent positive predictive value (86.8%) compared to B-mode ultrasound (76.1% and 77.2%) for detecting malignant lesions. In dense breasts, the specificity was even higher (92.8%). In breast lesions, malignancy creates a larger lesion on the elastogram than is seen on the routine grayscale B-scan image, presumed due to the desmoplastic reaction of the tumor and tethering in the adjacent tissue, as demonstrated in figure 16. In contrast, benign lesions are equal to or smaller than the grayscale image. Furthermore, a five-point scale utilized in some studies using Hitachi scanners characterizes the strain patterns and has shown promise for breast cancer diagnosis (Itoh *et al* 2006, Zhi *et al* 2010). Elastography therefore adds another imaging dimension, which can be used to help characterize indeterminate lesions such as solid-appearing cysts or solid hypoechoic well-circumscribed nodules (Burnside *et al* 2007, Svensson and Amiras 2006). Thus, it can potentially eliminate some unnecessary biopsies.

Unlike the breast, where elastography is used to characterize an already detected lesion, prostate elastography was developed to aid in detection of potential areas of prostate cancer, as grayscale ultrasound is relatively insensitive to identify discrete focal lesions. Practitioners in Austria (Pallwein *et al* 2008), Germany (Salomon *et al* 2008), Japan (Kamoi *et al* 2008) and the USA (Castaneda *et al* 2009) have shown improved detection of prostate cancer on average from less than 50% by ultrasound alone up to the 80% range using sonoelastography. Compression elastography on commercial equipment has been evaluated with respect to improving yield from a prostate biopsy. When larger lesions (greater than 5 mm) and lesions located in the peripheral regions are targeted, the biopsy yield improves (accuracy 76%), but has not been shown to be sufficient to replace blinded 10- or 12-core biopsies (Kamoi *et al* 2008).

Figure 16. Comparison B-scan, compression elastography and transient shear wave images of a breast with pathology confirmed invasive ductal carcinoma. The maximum diameter on the longitudinal axis on B-mode was 17 mm, whereas both elastographic techniques indicated a larger footprint of the cancer. (Courtesy of Dr W Svensson, Imperial College, London.)

All methods (compression and vibration) suffer from false positive findings due to benign prostatic hypertrophy with a false positive rate of about 20% (Castaneda *et al* 2009, Pallwein *et al* 2008).

A recent adaptation of compression elastography has been developed in the thyroid, using the gated pulsation of the carotid as the compressive force against the thyroid tissue. Dighe *et al*

have found an excellent correlation between tissue stiffness and papillary carcinoma, the most prevalent type of thyroid cancer. Benign nodules are significantly softer, so that, in a cohort of 59 patients, if elastography had been used in addition to grayscale features as a discriminator, as many as 60% of thyroid biopsies could have been safely deferred (Dighe *et al* 2010). Given the low prevalence and the indolence of most thyroid cancer, avoiding unnecessary biopsies may provide a great cost saving while permitting safe conservative management of thyroid nodules.

The newest application of elastography to clinical disease states involves vascular pathology, including assessment of thrombus age and overall vascular compliance (de Korte *et al* 2000, 2002, Biswas *et al* 2010, Weitzel *et al* 2009). Rubin *et al* have shown marked changes in stiffness of common femoral clots as they age (Xie *et al* 2004). This may potentially assist clinicians in deciding which thrombi require anticoagulation and for what time period. Direct measurement of vessel wall compliance would permit monitoring of blood pressure and the efficacy of antihypertensive therapy.

Many of the clinical applications attempted to date have been limited by their ability to adequately contact and displace tissue to achieve accurate and reproducible measurements. The next generation of imaging/elastography equipment is testing methods where ultrasound itself provides the tissue displacement, including acoustic radiation force imaging and vibroacoustography. The frequencies which acoustic radiation force imaging can achieve may permit more focused evaluation with improved resolution, especially important for detection of small lesions (prostate) or small displacements (vessels). Other potential future applications may include monitoring ablative therapies (radiofrequency ablation or cryoablation or high intensity focused ultrasound) in real time, as ablated tissues are many orders of magnitude stiffer than the background tissue (Zhang *et al* 2008a).

6. Discussion: future directions and unknowns

The previous section described some highly promising clinical applications that have been developed utilizing special technology for elastography. The near future will bring an expanding set of techniques, some integrated into scanners and others as stand-alone devices, with an expanding set of clinical diagnoses that benefit from an assessment of the biomechanical properties of tissues. However, some important areas have not received close attention and require dedicated effort to strengthen the foundations of elastography. Most importantly, we currently lack developmental models of diseases that link genetic, cellular, biochemical and gross pathological changes with observations of the biomechanical properties. For example, as cancer develops from less than 1 mm diameter to more than 1 cm, what is the evolution of the bio-mechanical properties at a macro scale, and how do they depend on the cellular level dynamics? Similar questions can be asked for other important targets such as the development of arterial plaques, liver fibrosis, prostate BPH, benign lesions of the breast and thyroid, blood clots, brain injuries and others. Some important foundational work has begun (Zhang *et al* 2008b, Carstensen *et al* 2008, Insana *et al* 2004, Kiss *et al* 2004, 2006, Sinkus *et al* 2005, Krouskop *et al* 1998, Barnes *et al* 2009, Samani *et al* 2007), but much remains to be studied. It is remarkable that clinical trials and technology development have been so successful given the paucity of understanding and data on the developmental aspects and mechanisms of altered biomechanics in specific disease states.

Another important direction for the field is the development of advanced estimators that go beyond relative stiffness and Young's modulus. Specifically, viscosity, anisotropy, nonlinearity, dispersion and their changes with disease have only recently been estimated and there is enormous opportunity for devising accurate estimation techniques and applying them

to developmental models of major diseases. The opportunity is great; however the challenges are also great, particularly since the study of elastographic imaging and the biomechanics of normal and diseased tissue is highly multidisciplinary, covering classical mechanics, wave propagation, biomechanics, imaging, digital signal processing, radiology and pathology plus other specialties. Progress will require highly interactive teams covering a broad range of expertise.

Acknowledgments

This work was supported by NIH grant 5R01AG02980-04. The authors are grateful for help from Ben Castenada, PhD, Zhe (Clark) Wu, PhD., and our other superb colleagues and co-authors over the past two decades. We also acknowledge some great insights and good humor over the years from Dr J Ophir, Dr J Bamber, and Dr A Sarvazyan.

References

Achenbach J D 1973 *Wave Propagation in Elastic Solids* (Amsterdam, The Netherlands: North Holland)

Adler R, Rubin J M and Bland P 1989 Characterization of transmitted motion in fetal lung: quantitative analysis *Med. Phys. Biol.* **16** 333–7

Adler R S, Rubin J M, Bland P H and Carson P L 1990 Quantitative tissue motion analysis of digitized M-mode images: gestational differences of fetal lung *Ultrasound Med. Biol.* **16** 561–9

Axel L and Dougherty L 1989 Heart wall motion: improved method of spatial modulation of magnetization for MR imaging *Radiology* **172** 349–50

Bamber J C, Barbone P E, Bush N L, Cosgrove D O, Doyely M M, Fueschsel F G, Meaney P M, Miller N R, Shiina T and Tranquart F 2002 Progress in freehand elastography of the breast *IEICE Trans Inf. Syst.* **E85D** 5–14

Bamber J C and Bush N L 1996 Freehand elasticity imaging using speckle decorrelation rate *Acoust. Imaging* **22** 285–92

Barbone P E and Gokhale N H 2004 Elastic modulus imaging: on the uniqueness and nonuniqueness of the elastography inverse problem in two dimensions *Inverse Probl.* **20** 283–96

Barnes S L, Young P P and Miga M I 2009 A novel model-gel-tissue assay analysis for comparing tumor elastic properties to collagen content *Biomech. Model. Mechaobiol.* **8** 337–43

Barr R G 2006 Clinical applications of real-time elastography technique in breast imaging *Proc. 5th Int. Conf. Ultrasonic Measurement Imaging Tissue Elasticity (8–10 Oct 2006, Snowbird, UT, USA)* p 51

Bercoff J, Tanter M and Fink M 2004 Supersonic shear imaging: a new technique for soft tissue elasticity mapping *IEEE Trans. Ultrason. Ferroelectr. Freq. Control* **51** 396–409

Berry G P, Bamber J C, Armstrong C G, Miller N R and Barbone P E 2006 Towards an acoustic model-based poroelastic imaging method: I. Theoretical foundation *Ultrasound Med. Biol.* **32** 547–67

Birnholz J C and Farrell E E 1985 Fetal lung development: compressibility as a measure of maturity *Radiology* **157** 495–8

Bishop J, Poole G and Plewes D B 1998 Magnetic resonance imaging of shear wave propagation in excised tissue *J. Magn. Reson. Imaging* **8** 1257–65

Bishop J, Samani A, Sciarretta J and Plewes D B 2000 Two-dimensional MR elastography with linear inversion reconstruction: methodology and noise analysis *Phys. Med. Biol.* **45** 2081–91

Biswas R, Patel P, Park D W, Cichonski T J, Richards M S, Rubin J M, Hamilton J and Weitzel W F 2010 Venous elastography: validation of a novel high-resolution ultrasound method for measuring vein compliance using finite element analysis *Semin. Dial.* **23** 105–9

Boursier J *et al* 2009 The combination of a blood test and fibroscan improves the non-invasive diagnosis of liver fibrosis *Liver Int.* **29** 1507–15

Bowen T 1981 Radiation-induced thermoacoustic soft tissue imaging *Proc. IEEE Ultrason. Symp. (14–16 Oct 1981, Chicago, IL, USA)* pp 817–22

Bowen T, Nasoni R L, Pifer A E and Sembroski G H 1981 Some experimental results on the thermoacoustic imaging of tissue equivalent phantom materials *Proc. IEEE Ultrason. Symp. (14–16 Oct 1981, Chicago, IL, USA)* pp 823–7

Burnside E S, Hall T J, Sommer A M, Hesley G K, Sisney G A, Svensson W E, Fine J P, Jiang J and Hangiandreou N J 2007 Differentiating benign from malignant solid breast masses with US strain imaging radiology *Radioliology* **245** 401–10

Carstensen E L, Parker K J and Lerner R M 2008 Elastography in the management of liver disease *Ultrasound Med. Biol.* **34** 1535–46

Castaneda B, Hoyt K, Westesson K, An L, Baxter L, Joseph J, Strang J, Rubens D and Parker K 2009 Performance of three-dimensional sonoelastography in prostate cancer detection: a comparison between *ex vivo* and *in vivo* experiments *Proc. IEEE Ultrason. Symp. (20–23 Sep 2009, Rome, Italy)* pp 519–22

Castéra L, Forns X and Alberti A 2008 Non-invasive evaluation of liver fibrosis using transient elastography *J. Hepatol.* **48** 835–47

Castéra L, Foucher J, Bernard P H, Carvalho F, Allaix D, Merrouche W, Couzigou P and de Lédinghen V 2010 Pitfalls of liver stiffness measurements: a 5-year prospective study of 13,369 examinations *Hepatology* **51** 828–35

Catheline S, Wu F and Fink M 1999 A solution to diffraction biases in sonoelasticity: the acoustic impulse technique *J. Acoust. Soc. Am.* **105** 2941–50

Chen S, Kinnick R, Greenleaf J F and Fatemi M 2007 Harmonic vibro-acoustography *IEEE Trans. Ultrason. Ferroelectr. Freq. Control* **54** 1346–51

Cox M and Rogers P H 1987 Automated noninvasive motion measurement of auditory organs in fish using ultrasound *J. Vib. Acoust. Stress Reliab. Des.* **109** 55–9

Curiel L, Souchon R, Rouviere O, Gelet A and Chapelon J Y 2005 Elastography for the follow-up of high-intensity focused ultrasound prostate cancer treatment: initial comparison with MRI *Ultrasound Med. Biol.* **31** 1461–8

Deffieux T, Gennisson J L, Muller M, Couade M, Bercoff J, Tanter M and Fink M 2007a The supersonic shear imaging as a quantitative tool for imaging *in vivo* liver stiffness *Proc. 6th Int. Conf. Ultrasonic Measurement Imaging Tissue Elasticity (2–5 Nov 2007, Santa Fe, NM, USA)* p 132

Deffieux T, Gennisson J L, Tanter M, Bercoff J and Fink M 2007b Mechanical muscle properties: transient elastography and 3D ultrasound ultrafast imaging *Proc. 6th Int. Conf. Ultrasonic Measurement Imaging Tissue Elasticity (2–5 Nov 2007, Santa Fe, NM, USA)* p 84

De Jong P G M, Arts T, Hoeks A P G and Reneman R S 1990 Determination of tissue motion velocity by correlation interpolation of pulsed ultrasonic echo signals *Ultrason. Imaging* **12** 84–98

de Korte C L, Carlier S G, Mastik F, Doyley M M, Van Der Steen A F W, Serruys P W and Bom N 2002 Morphological and mechanical information of coronary arteries obtained with intravascular elastography—feasibility study *in vivo Eur. Heart J.* **23** 405–13

de Korte C L, Pasterkamp G, Van Der Steen A F W, Woutman H A and Bom N 2000 Characterization of plaque components with intravascular ultrasound elastography in human femoral and coronary arteries *in vitro Circulation* **102** 617–23

Dickinson R J and Hill C R 1982 Measurement of soft tissue motions using correlation between A-scans *Ultrasound Med. Biol.* **8** 263–71

Dighe M, Kim J, Luo S and Kim Y 2010 Utility of ultrasound elastographic systolic thyroid stiffness index in reducing fine-needle aspirations *J. Ultrasound Med.* **29** 565–74

Doyley M M, Van Houten E E, Weaver J B, Poplack S, Duncan L, Kennedy F and Paulsen K D 2004 Shear modulus estimation using parallelized partial volumetric reconstruction *IEEE Trans. Med. Imaging* **23** 1404–16

Dresner M A, Rose G H, Rossman P J, Muthupillai R and Ehman R L 1998 Magnetic resonance elastography of the prostate *Radiology* **209P** 181

Eisensher A, Schweg-Toffer E, Pelletier G and Jacquemard G 1983 La palpation échographique rythmée-echosismographie *J. Radiol.* **64** 255–61

Emelianov S Y, Aglyamov S R, Shah J, Sethuraman S, Scott W G, Schmitt R, Motamedi M, Karpiouk A and Oraevesky A 2004 Combined ultrasound, optoacoustic and elasticity imaging *Proc. SPIE* **5320** 101–12

Esenaliev R O, Karabutov A A and Oraevsky A A 1999 Sensitivity of laser optoacoustic imaging in detection of small deeply embedded tumors *IEEE J. Sel. Top. Quantum. Electron.* **5** 981–8

Fahey B J, Nightingale K R, McAleavey S A, Palmeri M L, Wolf P D and Trahey G E 2005 Acoustic radiation force impulse imaging of myocardial radiofrequency ablation: initial *in vivo* results *IEEE Trans. Ultrason. Ferroelectr. Freq. Control* **52** 631–41

Fahey B J, Nightingale K R, Stutz D L and Trahey G E 2004 Acoustic radiation force impulse imaging of thermally- and chemically-induced lesions in soft tissues: preliminary *ex vivo* results *Ultrasound Med. Biol.* **30** 321–8

Fatemi M and Greenleaf J F 1998 Ultrasound-stimulated vibro-acoustic spectrography *Science* **280** 82–5

Fatemi M and Greenleaf J F 1999 Vibro-acoustography: an imaging modality based on ultrasound-stimulated acoustic emission *Proc. Natl Acad. Sci. USA* **96** 6603–8

Fatemi M, Wold L E, Alizad A and Greenleaf J F 2002 Vibro-acoustic tissue mammography *IEEE Trans. Med. Imaging* **21** 1–8

Fehrenbach J 2007 Influence of Poisson's ratio on elastographic direct and inverse problems *Phys. Med. Biol.* **52** 707–16

Fowlkes J B, Emelianov S Y, Pipe J G, Skovoroda A R, Carson P L, Adler R S and Sarvazyan A P 1995 Magnetic-resonance-imaging techniques for detection of elasticity variation *Med. Phys.* **22** 1771–8
Fung Y C 1984 *Biomechanics* (New York: Springer)
Gao L, Alam S K, Lerner R M and Parker K J 1995 Sonoelasticity imaging: theory and experimental verification *J. Acoust. Soc. Am.* **97** 3875–86
Gao L, Parker K J, Alam S K, Rubens D and Lerner R M 1997 Theory and application of sonoelasticity imaging *Int. J. Imaging Syst. Technol.* **8** 104–9
Gao L, Parker K J, Lerner R M and Levinson S F 1996 Imaging of the elastic properties of tissue—a review *Ultrasound Med. Biol.* **22** 959–77
Garra B S 2007 Imaging and estimation of tissue elasticity by ultrasound *Ultrasound Q.* **23** 255–68
Garra B S, Cespedes E I, Ophir J, Spratt S R, Zuurbier R A, Magnant C M and Pennanen M F 1997 Elastography of breast lesions: initial clinical results *Radiology* **202** 79–86
Ginat D T, Destounis S V, Barr R G, Castenada B, Strang J G and Rubens D J 2009 US elastography of breast and prostate lesions *Radiographics* **29** 2007–16
Greenleaf J F, Fatemi M and Insana M 2003 Selected methods for imaging elastic properties of biological tissues *Ann. Rev. Biomed. Eng.* **5** 57–78
Hall T J, Zhu Y N and Spalding C S 2003 *In vivo* real-time freehand palpation imaging *Ultrasound Med. Biol.* **29** 427–35
Hardy P A, Ridler A C, Chiarot C B, Plewes D B and Henkelman R M 2005 Imaging articular cartilage under compression-cartilage elastography *Magn. Reson. Imaging* **53** 1065–73
Holen J, Waag R C and Gramiak R 1985 Representation of rapidly oscillating structures on the Doppler display *Ultrasound Med. Biol.* **11** 267–72
Hoyt K, Castaneda B and Parker K J 2007a Muscle tissue characterization using quantitative sonoelastography: preliminary results *Proc. IEEE Ultrason Symp. (28–31 Oct 2007, New York, NY, USA)* pp 365–8
Hoyt K, Castaneda B and Parker K J 2008a Two-dimensional sonoelastographic shear velocity imaging *Ultrasound Med. Biol.* **34** 276–88
Hoyt K, Castaneda B, Zhang M, Nigwekar P, di Sant'Agnese P A, Joseph J V, Strang J, Rubens D J and Parker K J 2008b Tissue elasticity properties as biomarkers for prostate cancer *Cancer Biomarkers* **4** 213–25
Hoyt K, Kneezel T, Castaneda B and Parker K J 2008c Quantitative sonoelastography for the *in vivo* assessment of skeletal muscle viscoelasticity *Phys. Med. Biol.* **53** 4063–80
Hoyt K, Parker K J and Rubens D J 2007b Real-time shear velocity imaging using sonoelastographic techniques *Ultrasound Med. Biol.* **33** 1086–97
Huang S R, Lerner R M and Parker K J 1990 On estimating the amplitude of harmonic vibration from the Doppler spectrum of reflected signals *J. Acoust. Soc. Am.* **88** 2702–12
Huang S R, Lerner R M and Parker K J 1992 Time domain Doppler estimators of the amplitude of vibrating targets *J. Acoust. Soc. Am.* **91** 965–74
Insana M F, Pellot-Barakat C, Sridhar M and Lindfors K K 2004 Viscoelastic imaging of breast tumor microenvironment with ultrasound *J. Mammary Gland Biol. Neoplasia* **9** 393–404
Itoh A, Ueno E, Tohno E, Kamma H, Takahashi H, Shiina T, Yamakawa M and Matsumura T 2006 Breast disease: clinical application of US elastography for diagnosis *Radiology* **239** 341–50
Kallel F, Price R E, Konofagou E and Ophir J 1999 Elastographic imaging of the normal canine prostate *in vitro* *Ultrason. Imaging* **21** 201–15
Kamoi K, Okihara K, Ochiai A, Ukimura O, Mizutani Y, Kawauchi A and Miki T 2008 The utility of transrectal real-time elastography in the diagnosis of prostate cancer *Ultrasound Med. Biol.* **34** 1025–32
Kemper J, Sinkus R, Lorenzen J, Nolte-Ernsting C, Stork A and Adam G 2004 MR elastography of the prostate: initial *in-vivo* application *Rofo Fortschr. Geb. Rontgenstr. Neuen Bildgeb. Verfahr.* **176** 1094–9
Kennedy B F, Hillman T R, McLaughlin R A, Quirk B C and Sampson D D 2009 *In vivo* dynamic optical coherence elastography using a ring actuator *Opt. Express* **17** 21762–72
Kirkpatrick S J, Wang R K and Duncan D D 2006 OCT-based elastography for large and small deformations *Opt. Express* **14** 11585–97
Kiss M Z, Hobson M A, Varghese T, Harter J, Kliewer M A, Hartenbach E M and Zagaebski J A 2006 Frequency-dependent complex modulus of the uterus: preliminary results *Phys. Med. Biol.* **51** 3683–95
Kiss M Z, Varghese T and Hall T J 2004 Viscoelastic characterization of *in vitro* canine tissue *Phys. Med. Biol.* **49** 4207–18
Kolsky H 1953 *Stress Waves in Solids* (Oxford: Clarendon Press) (reprinted by (New York: Dover) 1963)
Konofagou E E and Hynynen K 2003 Localized harmonic motion imaging: theory, simulations and experiments *Ultrasound Med. Biol.* **29** 1405–13

Krouskop T A, Dougherty D R and Levinson S F 1987 A pulsed Doppler ultrasonic system for making noninvasive measurements of the mechanical properties of soft tissues *J. Rehabil. Res. Biol.* **24** 1–8

Krouskop T A, Wheeler T M, Kallel F, Garra B S and Hall T 1998 Elastic moduli of breast and prostate tissues under compression *Ultrason. Imaging* **20** 260–74

Kruse S A, Rose G H, Glaser K J, Manduca A, Felmlee J P, Jack C R and Ehman R L 2008 Magnetic resonance elastography of the brain *Neuroimage* **39** 231–7

Kruse S A, Smith J A, Lawrence A J, Dresner M A, Manduca A, Greenleaf J F and Ehman R L 2000 Tissue characterization using magnetic resonance elastography: preliminary results *Phys. Med. Biol.* **45** 1579–90

Lee F, Bronson J P, Lerner R M, Parker K J, Huang S R and Roach D J 1991 Sonoelasticity imaging: results in *in vitro* tissue specimens *Radiology* **181** 237–9

Lerner R M, Huang S R and Parker K J 1990 Sonoelasticity images derived from ultrasound signals in mechanically vibrated tissues *Ultrasound Med. Biol.* **16** 231–9

Lerner R M and Parker K J 1987 Sonoelasticity images derived from ultrasound signals in mechanically vibrated targets *Proc. 7th European Communities Workshop (Oct 1987, Nijmegen, The Netherlands)*

Lerner R M, Parker K J, Holen J, Gramiak R and Waag R C 1988 Sonoelasticity: medical elasticity images derived from ultrasound signals in mechanically vibrated targets *Acoust. Imaging* **16** 317–27

Levinson S F, Shinagawa M and Sato T 1995 Sonoelastic determination of human skeletal muscle elasticity *J. Biomech.* **28** 1145–54

Liang X, Adie S G, Renu J R and Boppart S A 2010 Dynamic spectral-domain optical coherence elastography for tissue characterization *Opt. Express* **18** 14183–90

Liang X, Oldenburg A L, Crecea V, Chaney E J and Boppart S A 2008 Optical micro-scale mapping of dynamic biomechanical tissue properties *Opt. Express* **16** 11052–65

Lorenzen J, Sinkus R, Schrader D, Lorenzen M, Leussler C, Dargatz M and Roschmann P 2001 Imaging of breast tumors using MR elastography *Rofo Fortschr. Geb. Rontgenstr. Neuen Bildgeb. Verfahr.* **173** 12–7

Manduca A, Dutt V, Borup D T, Muthupillai R, Greenleaf J F and Ehman R L 1998 An inverse approach to the calculation of elasticity maps for magnetic resonance elastography *Proc. SPIE* **3338** 426–36

Manduca A, Muthupillai R, Rossman P J, Greenleaf J F and Ehman R L 1996 Local wavelength estimation for magnetic-resonance elastography *Proc. IEEE Int. Conf. in Image Processing (16–19 Sep 1996, Lausanne, Switzerland)* pp 527–30

Manduca A, Oliphant T E, Dresner M A, Mahowald J L, Kruse S A, Amromin R, Felmlee J P, Greenleaf J F and Ehman R L 2001 Magnetic resonance elastography: non-invasive mapping of tissue elasticity *Med. Image Anal.* **5** 237–54

McAleavey S, Collins E, Kelly J, Elegbe E and Menon M 2009 Validation of SMURF estimation of shear modulus in hydrogels *Ultrason. Imaging* **31** 131–50

McAleavey S A and Menon M 2007 Direct estimation of shear modulus using spatially modulated acoustic radiation force impulses *Proc. IEEE Ultrason. Symp. (28–31 Oct 2007, New York, NY, USA)* p 558–61

McCracken P J, Manduca A, Felmlee J and Ehman R L 2005 Mechanical transient-based magnetic resonance elastography *Magn. Reson. Med.* **53** 628–39

McKnight A L, Kugel J L, Rossman P J, Manduca A, Hartmann L C and Ehman R L 2002 MR elastography of breast cancer: preliminary results *Am. J. Roentgenol.* **178** 1411–7

McLaughlin J, Parker K J, Renzi D and Wu Z 2007 Shear wave speed recovery using moving interference patterns obtained in sonoelastography experiments *J. Acoust. Soc. Am.* **121** 2438–46

Mitri F G, Davis B J, Greenleaf J F and Fatemi M 2009 *In vitro* comparative study of vibro-acoustography versus pulse-echo ultrasound in imaging permanent prostate brachytherapy seeds *Ultrasonics* **49** 31–8

Muthupillai R, Dutt V, Manduca A, Smith J A, Greenleaf J F and Ehman R L 1997 Resolution limits of MR elastography (MRE) *Radiology* **205** S 1386

Muthupillai R, Lomas D J, Rossman P J, Greenleaf J F, Manduca A and Ehman R L 1995 Magnetic resonance elastography by direct visualization of propagating acoustic strain waves *Science* **269** 1854–7

Nasoni R L, Liew S C, Halverson P G and Bowen T 1985 Thermoacoustic images generated by a 2450 MHz portable source and applicator *Proc. IEEE Ultrasonics Symp. (16–18 Oct 2005, San Francisco, CA, USA)* pp 899–904

Nightingale K R, Palmeri M L, Nightingale R W and Trahey G E 2001 On the feasibility of remote palpation using acoustic radiation force *J. Acoust. Soc. Am.* **110** 625–34

Nightingale K R, Zhai L, Dahl J J, Frinkley K D and Palmeri M L 2006 Shear wave velocity estimation using acoustic radiation force impulsive excitation in liver *in vivo Proc. IEEE Ultrason Symp. (3–6 Oct 2006, Vancouver, Canada)* pp 1156–60

Nightingale K, Nightingale R, Palmeri M and Trahey G 1999 Finite element analysis of radiation force induced tissue motion with experimental validation Proc. IEEE Ultrasonics Symp. (Lake Tahoe, NV, USA, 17-20 Oct.) pp 1319-23

O'Donnell M, Skovoroda A R, Shapo B M and Emelianov S Y 1994 Internal displacement and strain imaging using ultrasonic speckle tracking *IEEE Trans. Ultrason. Ferroelectr. Freq. Control* **41** 314–25

Oestricher H L 1951 Field and impedance of an oscillating sphere in a viscoelastic medium with an application to biophysics *J. Acoust. Soc. Am.* **23** 707–14

Ophir J, Alam S K, Garra B, Kallel F, Konofagou E, Krouskop T and Varghese T 1999 Elastography: ultrasonic estimation and imaging of the elastic properties of tissues *J. Eng. Med.* **213** (H3) 203–33

Ophir J, Cespedes I, Ponnekanti H, Yazdi Y and Li X 1991 Elastography: a quantitative method for imaging the elasticity of biological tissues *Ultrason. Imaging* **13** 111–34

Ophir J, Kallel F, Varghese T, Bertrand M, Céspedes I and Ponnekanti H 1997 Elastography: a systems approach *Int. J. Imaging Syst. Technol.* **8** 89–103

Oraevsky A A, Karabutov A A, Andreev V G and Esenaliev R O 1999 Laser optoacoustic imaging of the breast: detection of cancer angiogenesis *Proc. SPIE* **3597** 352–63

Pallwein L, Mitterberger M, Pinggera G, Aigner F, Pedross F, Gradl J, Pelzer A, Bartsch G and Frauscher F 2008 Sonoelastography of the prostate: comparison with systematic biopsy findings in 492 patients *Eur. J. Radiol.* **65** 304–10

Palmeri M L and Nightingale K R 2004 On the thermal effects associated with acoustic radiation force impulse imaging *IEEE Trans. Ultrason. Ferroelectr. Freq. Control* **51** 551–65

Palmeri M L, Wang M H, Frikley K D, Nightingale K R, Abdelmalek M F and Diehl A M 2007 Dependence of *in vivo*, radiation force derived hepatic shear modulus estimates on imaging approach: intercostal versus subcostal *Proc. IEEE Ultrason. Symp. (28–31 Oct 2007 New York, NY, USA)* pp 566–9

Parker K J, Gao L, Lerner R M and Levinson S F 1996 Techniques for elastic imaging: a review *IEEE Eng. Med. Biol. Mag.* **15** 52–9

Parker K J, Huang S R and Musulin R A 1990 Tissue response to mechanical vibrations for sonoelasticity imaging *Ultrasound Med. Biol.* **16** 241–6

Parker K J and Lerner R M 1992 Sonoelasticity of organs: shear waves ring a bell *J. Ultrasound Med.* **11** 387–92

Parker K J, Taylor L S, Gracewski S and Rubens D J 2005 A unified view of imaging the elastic properties of tissue *J. Acoust. Soc. Am.* **117** 2705–12

Patch S K and Scherzer O 2007 Guest editors' introduction: photo- and thermo-acoustic imaging *Inverse Probl.* **23** S1–10

Plewes D B, Betty I, Urchuk S N and Soutar I 1995 Visualizing tissue compliance with MR imaging *J. Magn. Reson. Imaging* **5** 733–8

Plewes D B, Bishop J, Samani A and Sciaretta J 2000 Visualization and quantification of breast cancer biomechanical properties with magnetic resonance elastography *Phys. Med. Biol.* **45** 1591–610

Righetti R, Kallel F, Stafford R J, Price R E, Krouskop T A, Hazle J D and Ophir J 1999 Elastographic characterization of HIFU-induced lesions in canine livers *Ultrasound Med. Biol.* **25** 1099–113

Rubens D J, Hadley M A, Alam S K, Gao L, Mayer R D and Parker K J 1995 Sonoelasticity of prostate cancer: *in vitro* results *Radiology* **195** 379–83

Sack I, Gedat E, Bernarding J, Buntkowsky G and Braun J 2004 Magnetic resonance elastography and diffusion-weighted imaging of the sol/gel phase transition in agarose *J. Magn. Reson.* **166** 252–61

Salomon G, Koellermann J, Thederan I, Chun F K H, Budeaus L, Schlomm T, Isbarn H, Heinzer H, Huland H and Graefen M 2008 Evaluation of prostate cancer detection with ultrasound real-time elastography: a comparison with step section pathological analysis after radical prostatectomy *Eur. Urol.* **54** 1354–62

Samani A, Bishop J, Luginbuhl C and Plewes D B 2003 Measuring the elastic modulus of *ex vivo* small tissue samples *Phys. Med. Biol.* **48** 2183–98

Samani A, Zubovits J and Plewes D 2007 Elastic moduli of normal and pathological human breast tissues: and inversion-technique-based investigation of 169 samples *Phys. Med. Biol.* **52** 1565–76

Sarvazyan A P, Rudenko O V, Swanson S D, Fowlkes J B and Emelianov S Y 1998 Shear wave elasticity imaging: a new ultrasonic technology of medical diagnostics *Ultrasound Med. Biol.* **24** 1419–35

Sarvazyan A P, Skovoroda A R, Emelianov S Y, Fowlkes J B, Pipe J G, Adler R S, Buxton R B and Carson P L 1995 Biophysical bases of elasticity imaging *Acoustical Imaging* vol 21 ed Jones J P (New York and London: Plenum Press) pp 223–40

Sato R, Fukusima A, Ichida N, Ishikawa H, Miwa H, Igarashi Y, Shimura T and Murakami K 1985 Nonlinear parameter tomography system using counterpropagating probe and pump waves *Ultrason. Imaging* **7** 49–59

Schmitt J M 1998 OCT elastography: imaging microscopic deformation and strain of tissue *Opt. Express* **3** 199–211

Sharma A C, Soo M S, Trehey G E and Nightingale K R 2004 Acoustic radiation force impulse imaging of *in vivo* breast masses *Proc. IEEE Ultrason. Symp. (24–27 Aug 2004, Montreal, Canada)* pp 728–31

Shiina T, Nitta N, Ueno E and Bamber J C 2002 Real time elasticity imaging using the combined autocorreclation method *J. Med. Ultrasonics* **29** 119–28

Sinkus R, Lorenzen J, Schrader D, Lorenzen M, Dargatz M and Holz D 2000 High-resolution tensor MR elastography for breast tumor detection *Phys. Med. Biol.* **45** 1649–64

Sinkus R, Siegmann K, Xydeas T, Tanter M, Claussen C and Fink M 2007 MR elastography of breast lesions: understanding the solid/liquid duality can improve the specificity of contrast-enhanced MR mammography *Magn. Reson. Med.* **58** 1135–44

Sinkus R, Tanter M, Xydeas T, Catheline S, Bercoff J and Fink M 2005 Viscoelastic shear properties of *in vivo* breast lesions measured by MR elastography *Magn. Reson. Imaging* **23** 159–65

Sugimoto T, Ueha S and Itoh K 1990 Tissue hardness measurement using the radiation force of focused ultrasound *Proc. IEEE Ultrason. Symp. (4–7 Dec 1990, Honolulu, HI, USA)* pp 1377–80

Sumi C 2008 Displacement vector measurement using instantaneous ultrasound signal phase—multidimensional autocorrelation and Doppler methods *IEEE Trans. Ultrason. Ferroelectr. Freq. Control* **55** 24–43

Svensson W E and Amiras D 2006 Ultrasound elasticity imaging *Breast Cancer Online* **9** e24 http://www.bco.org

Tanter M, Bercoff J, Athanasiou A, Deffieux T, Gennison J L, Montaldo G, Muller M, Tardivon A and Fink M 2008 Quantitative assessment of breast lesion viscoelasticity: initial clinical results using supersonic shear imaging *Ultrasound Med. Biol.* **34** 1373–86

Taylor K J 1976 Absolute measurement of acoustic particle velocity *J. Acoust. Soc. Am.* **59** 691–4

Taylor L S, Porter B C, Rubens D J and Parker K J 2000 Three-dimensional sonoelastography: principles and practices *Phys. Med. Biol.* **45** 1477–94

Taylor L S *et al* 2005 Prostate cancer: three-dimensional sonoelastography for *in vitro* detection *Radiology* **237** 981–5

Thomas A, Warm M, Hoopmann M, Diekmann F and Fischer T 2007 Tissue Doppler and strain imaging for evaluating tissue elasticity of breast lesions *Acad. Radiol.* **14** 522–9

Thitaikumar A, Krouskop T A, Garra B S and Ophir J 2007 Visualization of bonding at an inclusion boundary using axial-shear strain elastography: a feasibility study *Phys. Med. Biol.* **52** 2615–33

Tikkakoski T 2007 Magnetic resonance elastography of brain tumors *Acta Radiol.* **48** 249

Torr G R 1984 The acoustic radiation force *Am. J. Phys.* **52** 402–8

Tristam M, Barbosa D C, Cosgrove D O, Nassire D K, Bamber J C and Hill C R 1986 Ultrasonic study of *in vivo* kinetic characteristics of human tissues *Ultrasound Med. Biol.* **12** 927–37

Tristam M, Barbosa D C, Cosgrove D O, Nassiri D K, Bamber J C and Hill C R 1988 Application of Fourier analysis to clinical study of patterns of tissue movement *Ultrasound Med. Biol.* **14** 695–707

Urban M W, Silva G T, Fatemi M and Greenleaf J F 2006 Multifrequency vibro-acoustography *IEEE Trans. Med. Imaging* **25** 1284–95

Van Houten E E, Doyley M M, Kennedy F E, Weaver J B and Paulsen K D 2003 Initial *in vivo* experience with steady-state subzone-based MR elastography of the human breast *J. Magn. Reson. Imaging* **17** 72–85

Van Houten E E W, Miga M I, Weaver J B, Kennedy F E and Paulsen K D 2001 Three-dimensional subzone-based reconstruction algorithm for MR elastography *Magn. Reson. Med.* **45** 827–37

Van Houten E E W, Paulsen K D, Miga M I, Kennedy F E and Weaver J B 1999 An overlapping subzone technique for MR-based elastic property construction *Magn. Reson. Med.* **42** 779–86

Varghese T and Ophir J 1997 A theoretical framework for performance characterization of elastography: the strain filter *IEEE Trans. Ultrason. Ferroelectr. Freq. Control* **44** 164–72

Varghese T, Ophir J and Cespedes I 1996 Noise reduction in elastograms using temporal stretching with multicompression averaging *Ultrasound Med. Biol.* **22** 1043–52

Varghese T, Techavipoo U, Liu W, Zagzebski J A, Chen Q, Frank G and Lee F T Jr 2003 Elastographic measurement of the area and volume of thermal lesions resulting from radiofrequency ablation: pathologic correlation *Am. J. Roentgenol.* **181** 701–7

Von Gierke H E, Oestricher H L, Franke E K, Parrack H O and Von Wittern W W 1952 Physics of vibrations in living tissues *J. Appl. Physiol.* **4** 886–900

Wang J H, Changchien C S, Hung C H, Eng E L, Tung W C, Kee K M, Chen C H, Hu T H, Lee C M and Lu S N 2009 FibroScan and ultrasonography in the prediction of hepatic fibrosis in patients with chronic viral hepatitis *J. Gastroenterol.* **44** 439–46

Wang M H, Hedlund L W, Palmeri M L, Guy C D, Yang L, Diehl A M and Nightingale K R 2007 *In vivo* staging of liver fibrosis in a rat model using acoustic radiation force *Proc. IEEE Ultrason. Symp. (28–31 Oct 2007, New York, NY, USA)* pp 562–5

Wang R K, Ma A and Kirkpatrick S J 2006 Tissue Doppler optical coherence elastography for real time strain rate and strain mapping of soft tissue *Appl. Phys. Lett.* **89** 144103

Weaver J B, Doyley M, Cheung Y, Kennedy F, Madsen E L, Van Houten E E W and Paulsen K 2005 Imaging the shear modulus of the heel fat pads *Clin. Biomech.* **20** 312–9

Weaver J B, Van Houten E, Miga M I, Kennedy F E and Paulsen K D 2000 Three-dimensional steady state acquisition and reconstruction in MR elastography *Radiology* **217** 206

Weaver J B, Van Houten E E W, Miga M I, Kennedy F E and Paulsen K D 2001 Magnetic resonance elastography using 3D gradient echo measurements of steady-state motion *Med. Phys.* **28** 1620–8

Weitzel W F, Kim K, Henke P K and Rubin J M 2009 High-resolution ultrasound speckle tracking may detect vascular mechanical wall changes in peripheral artery bypass vein grafts *Ann. Vasc. Surg.* **23** 201–6

Wilson L S and Robinson D E 1982 Ultrasonic measurement of small displacements and deformations of tissue *Ultrason. Imaging* **4** 71–82

Wojcinski S, Farrokh A, Weber S, Thomas A, Fischer T, Slowinski T, Schmidtand W and Degenhardt F 2010 Multicenter study of ultrasound real-time tissue elastography in 779 cases for the assessment of breast lesions: improved diagnostic performance by combining the BI-RADS ®-US classification system with sonoelastography *Ultraschall Med.* **31** 484–91

Wu T, Felmlee J P, Greenleaf J F, Riederer S J and Ehman R L 2000 MR imaging of shear waves generated by focused ultrasound *Magn. Reson. Med.* **43** 111–5

Wu Z, Hoyt K, Rubens D J and Parker K J 2006 Sonoelastographic imaging of interference patterns for estimation of shear velocity distribution in biomaterials *J. Acoust. Soc. Am.* **120** 535–45

Wu Z, Taylor L S, Rubens D J and Parker K J 2002 Shear wave focusing for three-dimensional sonoelastography *J. Acoust. Soc. Am.* **111** 439–46

Wu Z, Taylor L S, Rubens D J and Parker K J 2004 Sonoelastographic imaging of interference patterns for estimation of the shear velocity of homogenous materials *Phys. Med. Biol.* **49** 911–22

Xie H *et al* 2004 Staging deep venous thrombosis using ultrasound elasticity imaging: animal model *Ultrasound Med. Biol.* **30** 1385–96

Yamakoshi Y, Sato J and Sato T 1990 Ultrasonic-imaging of internal vibration of soft-tissue under forced vibration *IEEE Trans. Ultrason. Ferroelectr. Freq. Control* **37** 45–53

Zerhouni E A, Parish D M, Rogers W J, Yang A and Shapiro E P 1988 Human heart: tagging with MR imaging—a method for noninvasive assessment of myocardial motion *Radiology* **169** 59–63

Zhai L, Madden J, Fu W C, Palmeri M L, Mouraviev V, Polaschik T and Nightingale K R 2010 Acoustic radiation force impulse imaging of human prostates *ex vivo Ultrasound Med. Biol.* **36** 576–88

Zhang M, Castenada B, Christensen J, Saad W E, Bylund K, Hoyt K, Strang J G, Rubens D J and Parker K J 2008a Real-time sonoelastography of hepatic thermal lesions in a swine model *Med. Phys.* **35** 4132–41

Zhang M, Castaneda B, Wu Z, Nigwekar P, Joseph J V, Rubens D J and Parker K J 2007a Congruence of imaging estimators and mechanical measurements of viscoelastic properties of soft tissues *Ultrasound Med. Biol.* **33** 1617–31

Zhang M, Nigwekar P, Castaneda B, Hoyt K, Joseph J V, di Sant'Agnese A, Messing E M, Strang J G, Rubens D J and Parker K J 2008b Quantitative characterization of viscoelastic properties of human prostate correlated with histology *Ultrasound Med. Biol.* **34** 1033–42

Zhang X, Zeraati M, Kinnick R, Greenleaf J F and Fatemi M 2007b Vibration mode imaging *IEEE Trans. Med. Imaging* **26** 843–52

Zhi H, Xiao X Y, Yang H Y, Ou B, Wen Y L and Luo B M 2010 Ultrasonic elastography in breast cancer diagnosis: strain ration versus 5-point scale *Acad. Radiol.* **17** 1227–33